Two-photon Resonance Enhanced MultiPhoton Ionization PhotoElectron Spectroscopy of the SH (SD) radical below and above the lowest ionization threshold.

Milan, J.B.; Buma, W.J.; de Lange, C.A.

DOI
10.1063/1.471850

Publication date
1996

Published in
Journal of Chemical Physics

Two-photon resonance enhanced multiphoton ionization photoelectron spectroscopy of the SH (SD) radical below and above the lowest ionization threshold

J. B. Milan, W. J. Buma, and C. A. de Lange
Laboratory for Physical Chemistry, University of Amsterdam, Nieuwe Achtergracht 127, 1018 WS Amsterdam, The Netherlands

(Received 29 May 1996; accepted 19 July 1996)

A two-photon resonance enhanced multiphoton ionization spectroscopic study on the mercapto radical is carried out in the one-photon energy region between 258 and 208 nm. Thirteen previously unobserved Rydberg states converging upon the $a\ ^1\Delta$ or $b\ ^1\Sigma^+$ excited ionic states are reported. Identification and characterization of several states with excitation energies below the lowest ionization limit are performed by analyses of the rotationally resolved two-photon excitation spectra, polarization studies, and photoelectron spectroscopy after excitation of the states. Detailed comparisons between the experimental and simulated excitation spectra, which show for three states clear indications of intensity anomalies, as well as the observation of multiple ionization channels demonstrate that for all states Rydberg–Rydberg and/or Rydberg–valence interactions determine the finer details of their electronic wave functions. Above the lowest ionization limit two-photon resonance enhancement is observed for six Rydberg states. These states are found to ionize by autoionization, rather than by absorption of a third photon. Remarkably, rotationally well-resolved excitation spectra can still be obtained for two of these states. Comparison of the dominant electronic configuration of the six Rydberg states allows us to explain these differences in terms of the possible autoionization channels. © *1996 American Institute of Physics.*
[S0021-9606(96)01540-1]

I. INTRODUCTION

The mercapto radical (SH) plays an important role in the ultraviolet photochemistry of sulfur-containing species released into the atmosphere from natural and anthropogenic sources. Moreover, as a result of the relatively high cosmic abundance of sulfur the molecule is also of interest from an astrophysical point of view.[1] Several sulfur-containing molecules such as CS, SO, OCS, and H_2S have already been detected in interstellar space,[2–4] but the simplest sulfur compound, i.e., SH, has not been observed yet.[5,6]

The $X\ ^2\Pi$ ground state of the SH radical has a $(1\sigma)^2(2\sigma)^2(3\sigma)^2(1\pi)^4(5\sigma)^2(2\pi)^3$ electronic configuration. Spin–orbit interaction [$A_0'' = -376.835\ \mathrm{cm}^{-1}$ (Ref. 7)] leads to an inverted splitting with the $^2\Pi_{3/2}$ state below the $^2\Pi_{1/2}$ state. The application of a wide range of techniques to study pure rotational and rovibrational transitions has led to a detailed elucidation of the spectroscopic properties of the $X\ ^2\Pi$ state.[8] The lowest excited state of the radical ($A\ ^2\Sigma^+$) arises from the valence excitation $5\sigma \rightarrow 2\pi$. Its spectroscopic and dynamic properties have been investigated and analyzed in several studies focusing on the $A\ ^2\Sigma^+ - X\ ^2\Pi$ electronic band system.[9–11]

Removal of an electron from the 2π molecular orbital, which consists essentially of the nonbonding $3p_x$ and $3p_y$ orbitals centered on the sulfur atom, gives rise to three different ionic states: the $X\ ^3\Sigma^-$ ground ionic state, and the $a\ ^1\Delta$ and $b\ ^1\Sigma^+$ excited ionic states. The higher-lying $A\ ^3\Pi$ and $c\ ^1\Pi$ excited ionic states derive from the removal of an electron from the 5σ molecular orbital. Ionization energies with an accuracy of 0.01 eV ($\sim 80\ \mathrm{cm}^{-1}$) are known from HeI vacuum ultraviolet (VUV) photoelectron spectroscopy (PES) measurements.[12] Recently, a more accurate determination of the ionization energy of the $X\ ^3\Sigma^-$ ground[13] and $a\ ^1\Delta$ excited[14] ionic states has been achieved by pulsed field ionization techniques. The spectroscopic properties of the majority of these states have been determined in several studies on the rotational and rovibrational transitions in the $X\ ^3\Sigma$ state,[15,16] as well as from analyses of the $A\ ^3\Pi - X\ ^3\Sigma^-$ and $c\ ^1\Pi - b\ ^1\Sigma^+$ band systems.[17–20] A recent zero-kinetic-energy pulsed-field ionization (ZEKE-PFI) study on the $a\ ^1\Delta$ excited ionic state of $SH^+(SD^+)$ has enabled the determination of the rotational parameters of the vibrationless level of this state.[14] A summary of the relevant spectroscopic parameters of these five ionic states is given in Table I. Apart from these experimental studies, the SH^+ ion has also been the subject of a number of theoretical studies investigating the electronic structure and spectroscopic properties of the ionic manifold.[21]

Returning to the electronic manifold of the neutral molecule, it will be clear that the higher excited states will consist of Rydberg states converging upon the various ionic limits. Until recently nine such states have been reported,[22,23] one of which has been identified as converging upon the $a\ ^1\Delta\ (v^+=0)$ excited ionic state. An early one-photon VUV absorption study has resulted in the determination of the spectroscopic parameters of seven electronic states.[22] In this study the D, F, G, and $H\ ^2\Pi$ states were fitted to a Rydberg series converging upon the ground ionic state, but the $C\ ^2\Delta$, $B\ ^2\Sigma$, and $E\ ^2\Sigma$ states were left unassigned. The assignment of all seven states has been reviewed on the basis of later *ab*

TABLE I. Spectroscopic constants (cm^{-1}) of the lower ionic states of SH^+ and SD^+.

Ionic state	Ionization energy	B_0	$D_0\times10^{-4}$	A_0	ω_e	$\omega_e x_e$
$SH^+X\ ^3\Sigma^-$	84 057.5[a]	9.134[b]	4.9[b]		2547.7	49.3[b]
$SD^+X\ ^3\Sigma^-$		4.733[b]	1.29[b]		1829.5	25.4[b]
$SH^+a\ ^1\Delta$	93 925[c]	9.187[c]	9.1[c]		$\nu_1-\nu_0=2450$[d,g]	
$SD^+a\ ^1\Delta$	93 944[c]	4.86[c]			g	
$SH^+b\ ^1\Sigma^+$	102 916[d,f]	9.164[e]	4.82[e]		$\nu_1-\nu_0=2450$[d,g]	
$SD^+b\ ^1\Sigma^+$	f				g	
$SH^+A\ ^3\Pi$	113 804[d]	7.477[b]	6.31[b]	−216.68[b]	1672.4	47.6[b]
$SD^+A\ ^3\Pi$		3.881[b]	1.68[b]	−216.52[b]	1200.9	24.5[b]
$SH^+c\ ^1\Pi$	126 548[d]	6.229[e]	6.64[e]			

[a]Reference 13.
[b]Reference 18.
[c]Reference 14.
[d]Reference 12.
[e]Reference 20.
[f]The ionization energies obtained in the present study for the $b\ ^1\Sigma^+$ ionic limit are: 102 754±80 cm^{-1} (SH^+) and 102 674±80 cm^{-1} (SD^+).
[g]Values obtained in the present study are given in Table III.

initio calculations on the vertical electronic spectrum of the mercapto radical, and suggestions have been put forward for a reassignment.[24]

The first (2+1) resonance enhanced multiphoton ionization (REMPI) study on the SH (SD) radical has been performed by Ashfold *et al.*[23] In this study three Rydberg states were observed, each deriving from a $2\pi\rightarrow4p$ electronic excitation. The analysis of the rotational fine structure accompanying the two-photon excitation enabled the assignment of the symmetries of the excited states and their spectroscopic parameters. Two of these states were identified as the first members of the $[X\ ^3\Sigma^-]np\sigma\ ^2\Sigma^-$ and $[X\ ^3\Sigma^-]np\pi\ ^2\Pi$ Rydberg series converging upon the ground ionic state, while the third state was recognized as a $^2\Phi$ state built upon an excited ionic core. This state was reasoned to derive from the $[a\ ^1\Delta]4p\pi$ configuration. It was shown that the $^2\Sigma^-$ state corresponded to the state previously observed in the one-photon VUV work,[22] where it had been assigned erroneously to $C\ ^2\Delta$.

From the observation that the $a\ ^1\Delta$ and $b\ ^1\Sigma^+$ excited ionic states only lie 1.22 and 2.34 eV above the $X\ ^3\Sigma^-$ ground ionic state (see Table I), respectively, it is clear that the Rydberg states built upon these ionic cores are energetically not very distant from the Rydberg states converging upon the $X\ ^3\Sigma^-$ ground ionic state, and should be easily accessible by means of two-photon excitation spectroscopy. In fact, *ab initio* calculations indicate where such states are expected in the vertical electronic spectrum.[24] Spectroscopic studies of the electronic and dynamic properties of these ''excited core'' Rydberg states are of considerable interest from several points of view. On the one hand, they might serve as a stepping stone for the generation of excited SH^+ (SD^+) ions in well-defined single (ro)vibronic states. On the other hand, such Rydberg states will be located below as well as above the lowest ionic threshold. Comparison of the characteristics of the states below and above this threshold should enable a detailed unraveling of autoionization processes. Finally, SH is isovalent with OH, an extremely important radical in combustion, atmospheric, and interstellar chemistry. High-resolution multiphoton spectroscopy of excited core Rydberg states of this radical is virtually impossible as a result of the high ionization energies of the ionic states. Studies of excited core Rydberg states in SH might thus shed some light on the electronic and dynamic properties of such states in OH.

It is in this spirit that we have initiated an extensive study of Rydberg states built upon excited ionic cores in SH (SD). In this work, Rydberg states are detected and characterized by two-photon resonance enhanced multiphoton ionization spectroscopy in combination with mass-resolved ion detection, and, in particular, high-resolution photoelectron spectroscopy. As will become apparent the application of photoelectron spectroscopy to these Rydberg states is a prerequisite for a fundamental characterization of the electronic composition of the states and their photoionization dynamics.

SH (SD) radicals are obtained in our studies by *in situ* photodissociation of H_2S (D_2S) following excitation to its first dissociative absorption band which spans the wavelength range from 270 to 180 nm.[25] The photofragmentation of H_2S (D_2S) has been the subject of a large number of investigations in which the spin–orbit, vibrational, and rotational state distributions of the SH (SD) fragments in their ground state have been measured for several photodissociation wavelengths.[26–33] It has been shown that after photodissociation of H_2S (D_2S), using various near-ultraviolet photodissociation wavelengths, SH (SD) fragments are formed in their ground vibronic level with a ~3:2 ratio over the $^2\Pi_{3/2}$ and $^2\Pi_{1/2}$ spin–orbit components, and with a rotational distribution over each of these components which can be char-

acterized by a Boltzmann temperature of ~300 K. In the present study H_2S (D_2S) photodissociation and SH (SD) two-photon resonance enhanced multiphoton ionization are carried out with identical near-ultraviolet excitation wavelengths between 258 and 208 nm.

Employing the above approach we have been able to investigate 14 Rydberg states of SH (SD) which had not been observed before. In a number of publications we have already reported on the spectroscopic properties and/or photoionization dynamics of two of these states.[14,34,35] The $n=5$ member of the $[a\ ^1\Delta]np\pi\ ^2\Phi$ series, of which $n=4$ had been previously studied, was shown to have several unusual properties.[34] Despite the fact that its excitation energy exceeds the lowest ionization threshold, rotationally well-resolved and analyzable excitation spectra could be obtained. The photoelectron spectra measured after excitation of this state revealed that ionization occurs by the absorption of a third photon after the two-photon excitation step, rather than through autoionization into the ionization continua of the $X\ ^3\Sigma^-$ ground ionic state. These results were explained by a slow autoionization mechanism.

High-resolution photoelectron spectroscopy enabled us to study the photoionization dynamics of the $[a\ ^1\Delta]3d\pi^2\Phi$ excited state[35] whose two-photon excitation spectrum will be discussed and analyzed in detail in the present paper. The combination with high-quality *ab initio* calculations in this case allowed a detailed unraveling of the photoionization dynamics. Both the experimental and calculated spectra showed a strong asymmetry in the rotational ionic branching ratios and provided a clear example of a situation in which the classical picture of photoionization is no longer adequate. The need for a quantum-mechanical picture was also apparent from the observation that photoionization occurred only with a change in angular momentum up to $\Delta N=\pm 2$, whereas transitions up to $\Delta N=\pm 4$ were expected on the basis of photoionization selection rules. The same Rydberg state has also been used in a ZEKE-PFI experiment on the $a\ ^1\Delta$ ionic state.[14] Apart from providing an accurate ionization threshold and rotational parameters for this state, this study showed that high-n Rydberg states built upon the $a\ ^1\Delta$ ionic core are relatively insensitive to electronic and rotational autoionization processes.

The subject of the present paper is the observation and characterization of all states investigated up until now, except the $[a\ ^1\Delta]5p\pi^2\Phi$ state. An energy-level diagram depicting the excitation energies and electronic configurations of these 13 previously unobserved Rydberg states is given in Fig. 1. The sections in which these states will be discussed are included as well in Fig. 1. Seven of these states have an excitation energy below the lowest ionization limit. Photoelectron spectra via these states show unambiguously that they are members of various Rydberg series with the $a\ ^1\Delta$ or $b\ ^1\Sigma^+$ ionic state as their dominant ionic core configuration. It will be shown that several perturbations must be invoked to understand the anomalies observed in recorded two-photon excitation spectra and the $a\ ^1\Delta{:}b\ ^1\Sigma^+$ ratio in their photoelectron spectra. The present work also includes the study of six other Rydberg states with excitation energies exceeding the lowest ionization threshold. Despite this fact we could observe rotationally resolved excitation spectra for two of these states. The results elucidate the intrinsic details and importance of the various autoionization channels available for Rydberg states built upon different excited ionic cores.

II. EXPERIMENT

Two kinds of experiments were performed. In the first type excited states were located by scanning the excitation wavelength, while simultaneously monitoring either the SH^+ (SD^+) ion channel or an energy-selected part of the electron current. Subsequently, the photoelectrons were analyzed at a fixed excitation wavelength according to their kinetic energies.

A detailed description of the employed ''magnetic-bottle'' spectrometer has been reported elsewhere.[36] Ground-state SH (SD) radicals were produced *in situ* by photolysis of H_2S (D_2S) via excitation to the first dissociative absorption band. A single excimer-pumped dye laser provided photons both for the photolysis and the subsequent two-photon resonant multiphoton ionization (MPI) spectroscopy of the SH (SD) radicals. The laser system consists of a Lumonics HyperDye-500 dye laser (bandwidth ~0.08 cm^{-1}) operating on C500, C480, C460, Exalite440, and MSB, which is pumped by a XeCl excimer laser (Lumonics HyperEx-460) operating at 30 Hz. The dye laser output is frequency doubled using a Lumonics Hypertrak-1000 unit equipped with a BBO or KDP crystal. The output, which is polarized parallel to the time-of-flight axis of the spectrometer and has a pulse width of about 10 ns, is focused into the magnetic-bottle spectrometer using a quartz lens with a focal length of 25 mm. In order to avoid space-charge effects, the laser power was kept as low as possible. The polarization of the excitation light could be changed from linear to circular by means of a homemade Fresnel rhomb. For calibration of both the wavelengths and the photoelectron kinetic energies, resonances of xenon and atomic sulfur [which is also produced by the photolysis of H_2S (D_2S) and SH (SD)], in the two-photon energy range of 79 500–89 800 cm^{-1} were used.[37,38]

In the present study photodissociation and REMPI spectroscopy are performed with the same laser. The concentration of SH (SD) radicals might therefore depend on the employed excitation wavelength. However, the SH (SD) concentration is expected to be a slowly varying function of the wavelength, allowing for the comparison of intensities of signals within a limited excitation interval, say 1000 cm^{-1} or less.

H_2S (99.6% Messer Griesheim) and D_2S (98%*D*, Campro Scientific) were used without further purification. Each was introduced into the spectrometer, in turn, as a continuous effusive ''leak.''

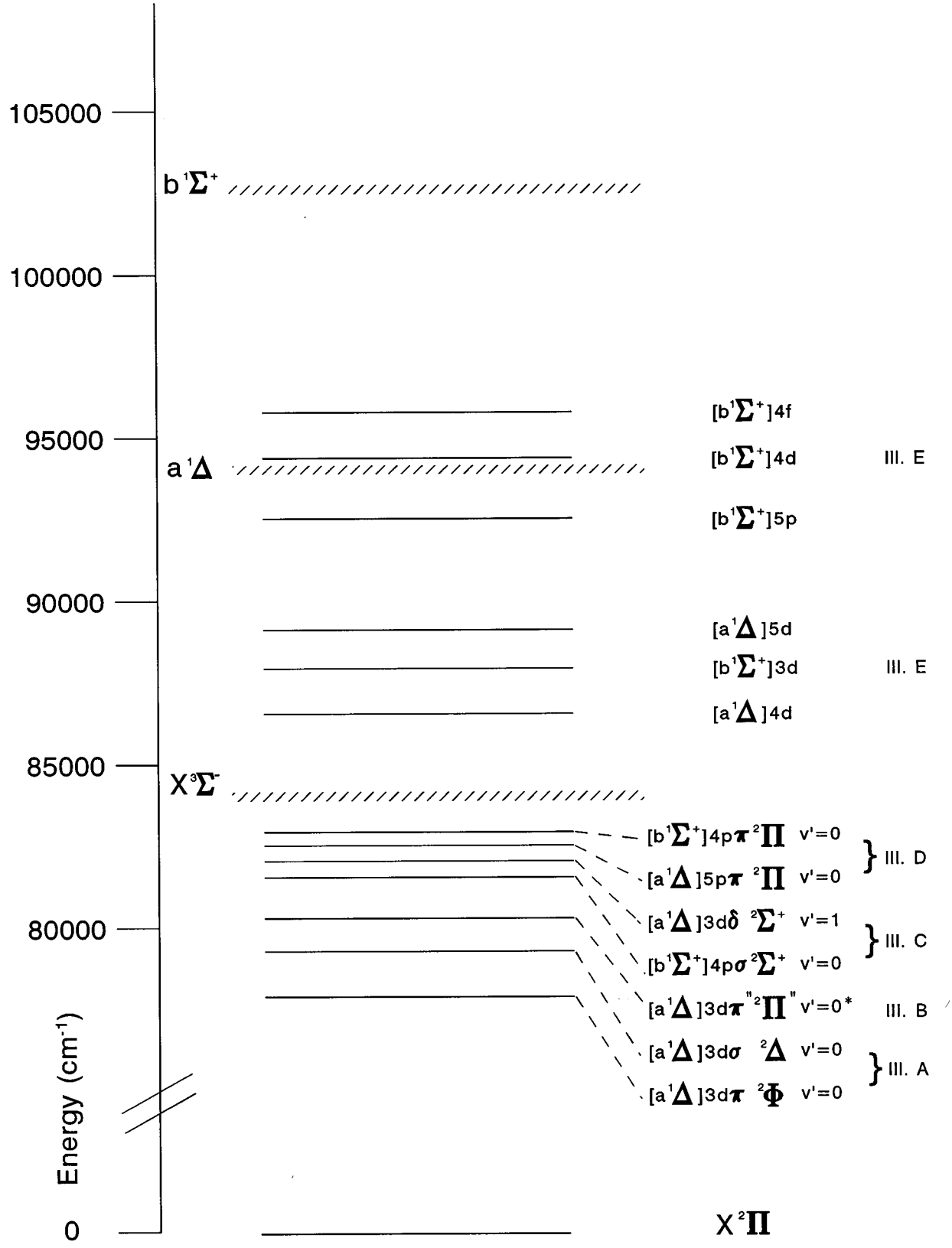

FIG. 1. Energy-level diagram showing the 13 newly observed Rydberg states of SH and the relevant ionization limits. Most of these states have also been observed for SD. The state marked with an asterisk was only seen for SD. The section in which each of these states is discussed is indicated at the right-hand side.

III. RESULTS AND DISCUSSION

A. Excitation spectra between 77 500 and 78 500 cm^{-1}

Figures 2(a) and 2(c) show the two-photon excitation spectra of the SH and SD radicals in the two-photon range of 77 500–78 500 cm^{-1} obtained by monitoring only photoelectrons with a kinetic energy of about 2.9 eV. Both spectra consist of two subbands whose energy separations correspond well with the spin–orbit splitting of the $X\ ^2\Pi$ ground state [$A_0''(SH) = -376.835\ cm^{-1}$ (Ref. 7), $A_0''(SD) = -376.75\ cm^{-1}$ (Ref. 10)]. From the small isotope shift in going from SH [Fig. 2(a)] to SD [Fig. 2(c)] it can be concluded that the vibrational quantum number does not change upon excitation, i.e., the excitation involves a 0–0 transition. This conclusion is supported by the photoelectron spectrum (Fig. 3).

Figure 3 depicts the photoelectron spectrum obtained for (2+1) ionization via the S_2 (5/2) rotational line at a one-photon energy of 38 958 cm^{-1}. The photoelectrons with a kinetic energy of 2.9 eV in Fig. 3 derive from a photoionization process in which the ground state $X\ ^2\Pi\ (v''=0)$ SH radical absorbs three photons and is ionized into the $a\ ^1\Delta$ ionization continua of the SH^+ ion. The remaining three photoelectron peaks in Fig. 3 can be attributed to a three-photon ionization process of atomic sulfur in which the $^3P_2$ ground state ionizes into the $^4S^o$ (4.13 eV), $^2D^o$ (2.29 eV), and $^2P^o$ (1.09 eV) ionization continua via the two-photon resonant $6p\ ^3P_1$ state.[38] These peaks serve as a direct internal kinetic energy calibration for the photoelectrons originating from the SH radical. Figure 3 thus allows for a definite assignment of the ionic core associated with the observed Rydberg state as the excited $a\ ^1\Delta\ (v^+=0)$ state. Figure 3 also shows that ionization only occurs to this particular $a\ ^1\Delta$ level; no photoelectron peaks corresponding to ionization to higher vibrational levels of the $a\ ^1\Delta$ state, nor to the energetically allowed $X\ ^3\Sigma^-$ and $b\ ^1\Sigma^+$ ionic states are observed.

Rotational analyses of the two-photon excitation spectra shown in Figs. 2(a) and 2(c) have been performed using combination differences based upon the well-known rotational constants of the $X\ ^2\Pi$ ground state and the calculation of rotational line strengths. The latter have been obtained by inserting the wave functions for both the ground and excited states, expressed in parity-conserving Hund's case (a) bases, and matrix elements derived using a conventional linear molecule Hamiltonian,[39] into the appropriate expression for the two-photon transition probability.[40] The comparison of experimental with simulated excitation spectra for several excited-state symmetries led to the unambiguous conclusion that the excited state must be of $^2\Phi$ symmetry. This conclusion is supported by the absence of transitions to excited state levels with $J' \leqslant 3/2$ in either excitation spectrum, and by the observation that the relative intensities of the various rotational branches can be reproduced reasonably well with the $T^2_{\pm 2}$ component of the two-photon transition tensor. The spectral parameters obtained from the least-squares fit to the observed line positions are given in Table II, while the simulated spectra based upon these constants are depicted in Figs. 2(b) and 2(d) for SH and SD, respectively.

The lowest Rydberg state of $^2\Phi$ symmetry expected in the vertical electronic spectrum of SH (SD) arises from the $[a\ ^1\Delta]4p\pi$ configuration and has been observed at 9.14 eV in a previous (2+1) REMPI study.[23] Calculations predict that the second $^2\Phi$ state should arise from the $[a\ ^1\Delta]3d\pi$ configuration[24] and is expected to lie some 0.6 eV higher in energy. Our newly observed $^2\Phi$ resonance at 9.67 eV agrees well with this expectation. All of the transitions identified in previous one-photon VUV absorption studies and in (2+1) REMPI studies[22,23,34] indicate that the highest occupied 2π molecular orbital in the ground state is to a major extent composed of the $3p_{x,y}$ orbitals on the sulfur atom. Our observation of a two-photon transition to the $[a\ ^1\Delta]3d\pi\ ^2\Phi$ state would consequently seem to be at odds with the atomic Laporte selection rule for two-photon excitation ($\Delta l = 0, \pm 2$). *Ab initio* calculations have shown, however, that the $3d\pi$ orbital of the $[a\ ^1\Delta]3d\pi\ ^2\Phi$ state has some p (5.04%) and f (0.39%) character as well.[35] These contributions would make the two-photon transition to the $[a\ ^1\Delta]3d\pi\ ^2\Phi$ state somewhat allowed.

The simulated spectra displayed in Figs. 2(b) and 2(d) show reasonable overall agreement with the measured spectra. A more detailed comparison of the experimental and calculated intensities, however, indicates that the two spectra show small differences. First, the Q_1 and S_1 rotational branches in the experimental excitation spectra have slightly larger and smaller intensities, respectively, than predicted by the two-photon rotational line strength calculations. Second, the intensities of the higher members of the S_1 branch decrease faster in the experimental spectra than in the theoretical ones. Third, the $^sR_{21}$ rotational branch in the SD spectrum has a larger intensity than predicted.

Inspection of the parameters derived from the rotational analyses reveals another noteworthy point. *A priori* one would expect that for the $[a\ ^1\Delta]3d\pi$ Rydberg configuration the dominant contribution to the spin–orbit parameter A would arise from the spin–orbit coupling of the single $3d\pi$ electron, and that therefore this parameter would be small and positive. The observation that the experimentally derived value is negative is at odds with such expectations.

One possible explanation for the fast decline of the intensity in the S_1 rotational branch could be found in the presence of heterogeneous predissociation, whose importance might in principle be determined from linewidth measurements. However, since the linewidths in the present measurements are to a large extent determined by power and/or saturation broadening effects, we cannot assess the influence of predissociation very well. Power broadening effects were virtually unavoidable for all recorded two-photon excitation spectra, since both the production of SH (SD) radicals and the resonance enhanced multiphoton ionization probability are reduced by lowering the laser power. Saturation of the two-photon excitation step would not only broaden the lines, but would also have an effect on the relative line strenghts. On the other hand, even if predissociation or saturation would play a significant role, they could not explain all ob-

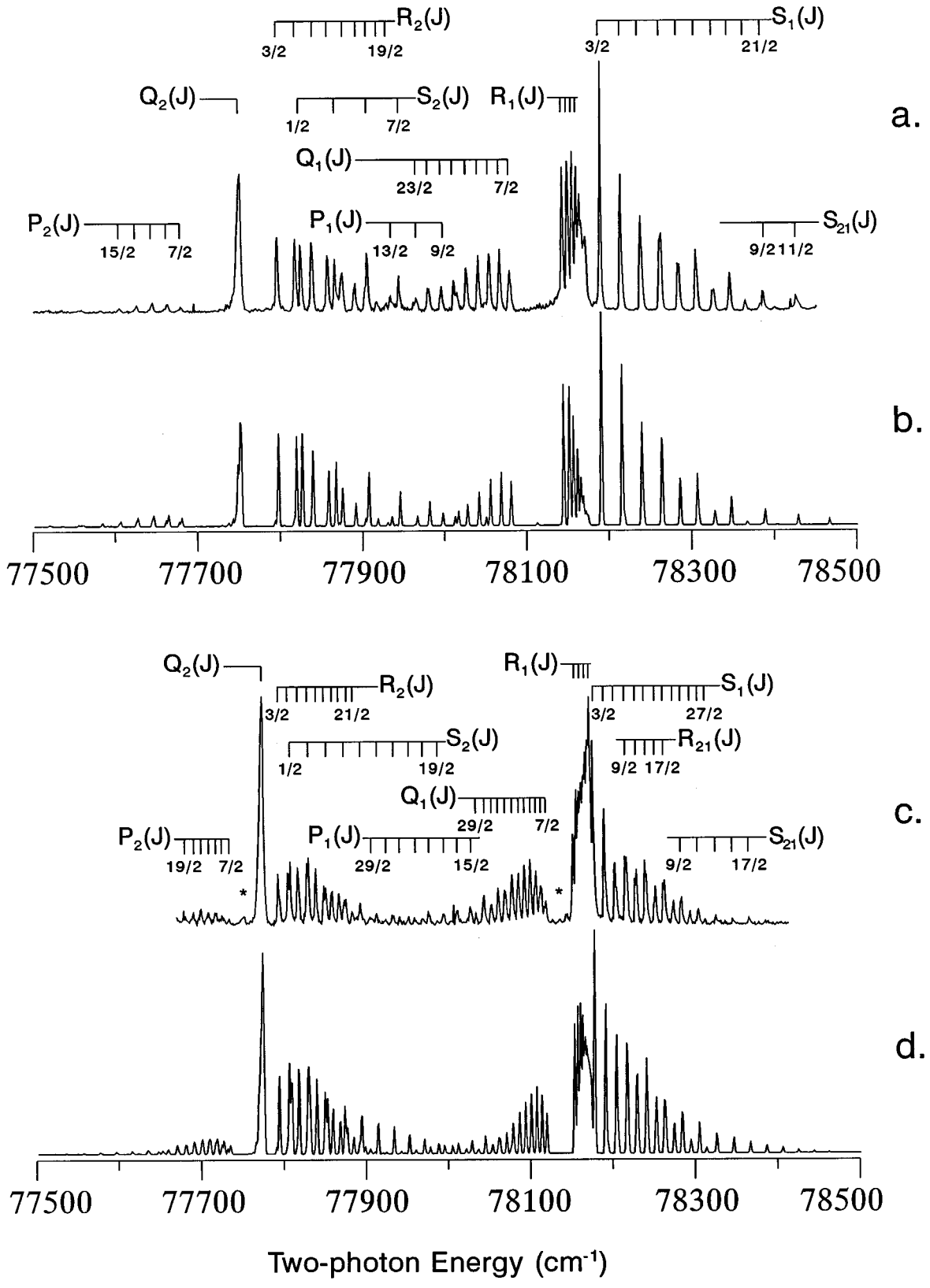

FIG. 2. (a) Experimental two-photon excitation spectrum of the $[a\ ^1\Delta]3d\pi\ ^2\Phi\ (v'=0)\leftarrow\leftarrow X\ ^2\Pi\ (v''=0)$ transition in SH. Individual line assignments are given by the combs above the spectrum. (b) Simulated excitation spectrum for SH using the spectroscopic constants given in Table II and a Gaussian linewidth of 2 cm^{-1}. (c) Experimental two-photon excitation spectrum of the $[a\ ^1\Delta]3d\pi\ ^2\Phi\ (v'=0)\leftarrow\leftarrow X\ ^2\Pi\ (v''=0)$ transition in SD. The resonances marked with an asterisk do not derive from SD but from SH impurities. (d) Simulated excitation spectrum for SD. Spectra (a) and (c) were obtained with electron detection.

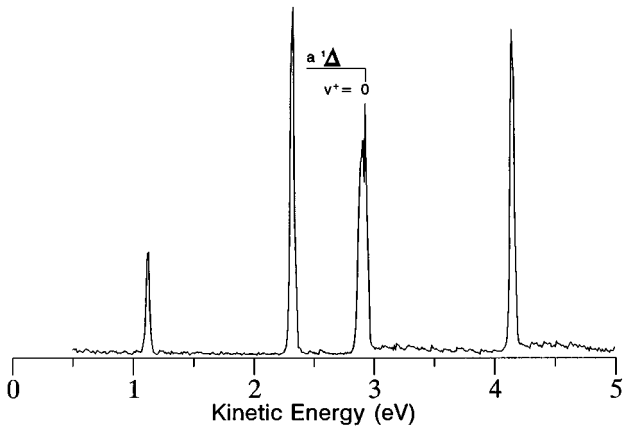

FIG. 3. Photoelectron spectrum obtained for (2+1) ionization via the S_2 (5/2) rotational transition to the $[a\ ^1\Delta]3d\pi\ ^2\Phi$ ($v'=0$) state of SH. The peaks not marked in the figure derive from ionization of sulfur atoms and serve as an internal calibration.

served intensity differences between experiment and theory.

Other possible explanations for the intensity anomalies can be found in the influence of the ground state population of the SH (SD) radical or the resonance enhancement of the MPI process employed here. In simulating the spectra we assumed an isotropic molecular sample whose overall population in the $^2\Pi_{3/2}$ and $^2\Pi_{1/2}$ spin–orbit states of SH (SD) is in the ratio 3:2, and whose rotational distribution over each of these states is characterized by a Boltzmann temperature of 300 K.[32] Deviations from the above distribution over spin–orbit and rotational states, however, cannot explain intensity anomalies between different rotational branches originating from one ground state spin–orbit component. Effects of ground state alignment in the SH (SD) fragments as a result of the H_2S (D_2S) photodissociation step can be regarded as insignificant, as shown by our studies on the photoionization dynamics via the $[a\ ^1\Delta]3d\pi\ ^2\Phi$ state.[35]

In a (2+1) REMPI process the intensity of a MPI transition is proportional to the product of the two-photon cross section for excitation to the excited state level from the ground state, and the one-photon ionization cross section from the upper level. In this multiphoton ionization process deviations from the expected intensities can arise from interference effects resulting from a near resonance at the one-photon level as well as from interaction between states at the resonant two-photon level. The two-photon excitation spectrum of NO provides several nice examples in which the observed rotational structure could only be accounted for if the contribution of one-photon near-resonant intermediate states was taken into consideration.[41–43] For example, the $C\ ^2\Pi \leftarrow\leftarrow X^2\Pi$ two-photon excitation spectrum was found to be dominated by Q branches as a consequence of the major contribution of the one-photon near-resonant $A\ ^2\Sigma^+$ state in the two-photon transition amplitude.[41] The validity of such an explanation in the present case is however questionable, bearing in mind that there are only a limited number of possible candidates for near resonance at the one-photon level whose configurations differ only by one electron from the two-photon resonant $[a\ ^1\Delta]3d\pi\ ^2\Phi$ Ryd-

TABLE II. Spectroscopic constants (cm^{-1}) derived in the present study for various Rydberg states of SH and SD. For comparison the spectroscopic constants of the $X\ ^2\Pi$ ground state are given as well.[a,b] The values in parentheses represent the standard deviation in the last significant digits.

	Electronic state	T_v	B_v	$D_v\times10^{-4}$	A_v	γ_v
SH	$X\ ^2\Pi(v''=0)$	0	9.604	4.8299	−376.835	
SH	$[a\ ^1\Delta]3d\pi\ ^2\Phi(v'=0)$	78 006.36 (9)	8.855 (3)	2.9 (2)	−1.18(6)	
SH	$[a\ ^1\Delta]3d\sigma\ ^2\Delta(v'=0)$	79 652±80				
SH	$[b\ ^1\Sigma^+]4p\sigma\ ^2\Sigma^+(v'=0)$	81 692.80 (45)	8.609(28)	−19 (3)		0.30(7)
SH	$[a\ ^1\Delta]3d\delta\ ^2\Sigma^+(v'=1)$	82 287.65 (67)	8.214(34)	−15 (4)		
SH	$[a\ ^1\Delta]5p\pi\ ^2\Pi(v'=0)$	82 766±80				
SH	$[b\ ^1\Sigma^+]4p\pi\ ^2\Pi(v'=0)$	83 189±30				
SH	$[a\ ^1\Delta]4d$ complex	86 816±20				
SH	$[b\ ^1\Sigma^+]3d$ complex	88 017±30				
SH	$[a\ ^1\Delta]5d$ complex	89 318±20				
SH	$[b\ ^1\Sigma^+]5p$ complex	92 720±30				
SH	$[b\ ^1\Sigma^+]4d$ complex	94 571±30				
SH	$[b\ ^1\Sigma^+]4f$ complex	95 620±30				
SD	$X\ ^2\Pi(v''=0)$	0	4.900	1.35	−376.75	
SD	$[a\ ^1\Delta]3d\pi\ ^2\Phi(v'=0)$	77 996.65 (12)	4.668 (3)	9.79 (15)	−1.25(7)	
SD	$[a\ ^1\Delta]3d\sigma\ ^2\Delta(v'=0)$	79 634±80				
SD	$[a\ ^1\Delta]3d\pi''\ ^2\Pi''(v'=0)$	80 420.6 (3)	4.342 (7)	−3.1 (3)		
SD	$[a\ ^1\Delta]3d\delta\ ^2\Sigma^+(v'=1)$	81 451.36 (13)	4.576 (9)	10 (1)		0.14(4)
SD	$[b\ ^1\Sigma^+]4p\sigma\ ^2\Sigma^+(v'=0)$	81 946.7 (3)[c]	4.47 (1)[c]	−4.6 (7)[c]		
SD	$[b\ ^1\Sigma^+]4p\pi\ ^2\Pi(v'=0)$	82 814±30				
SD	$[a\ ^1\Delta]5p\pi\ ^2\Pi(v'=0)$	82 964±30				
SD	$[a\ ^1\Delta]4d$ complex	86 816±20				
SD	$[a\ ^1\Delta]5d$ complex	89 318±20				

[a]Reference 7.
[b]Reference 10.
[c]The validity of these parameters should be taken with caution (see the text for further detail).

berg state. In fact, only the $[a\ ^1\Delta]6\sigma^*\ ^2\Delta$ valence state and the $[a\ ^1\Delta]4s\ ^2\Delta$ Rydberg state would fulfill such requirements, but their calculated excitation energies of 7.07 and 8.31 eV,[24] respectively, are so high that one could hardly consider them near resonant.

An explanation which seems more likely and has been amply demonstrated in absorption and emission studies of several other diatomics[44–49] involves the interaction with another state at the resonant level. Studies on NO, for example, have shown that a strong interaction between the $3d\sigma H\ ^2\Sigma^+$ and the $3d\pi H'\ ^2\Pi$ states caused by l uncoupling ultimately leads to the total annihilation of the fully allowed R rotational branch of the $A\ ^2\Sigma^+(v''=2)\rightarrow H'\ ^2\Pi(v'=2)$ band.[49] Intensity anomalies between different rotational branches in one-photon studies are usually ascribed to a quantum mechanical interference between two different transition moments of comparable strength, due to the interaction between rovibrational manifolds with different electronic symmetries. In two-photon spectroscopy the interference between two different two-photon transition moments of comparable magnitude may similarly influence the intensity distribution between the allowed rotational branches of a two-photon transition. In fact, it was on this basis that in two previous $(2+1)$ REMPI studies on two other Rydberg states of SH (SD) of $^2\Phi$ symmetry,[23,34] arising from the $[a\ ^1\Delta]4p\pi$ and $[a\ ^1\Delta]5p\pi$ configurations, l uncoupling was invoked. The excitation spectra of both states showed similar intensity anomalies as observed here, while for the $[a\ ^1\Delta]5p\pi\ ^2\Phi$ state an equally unexpected negative value for A was derived. In these studies further substantiation of l uncoupling could not be pursued, since the spectroscopic properties of the perturbing states were not known. In the present study, however, we do have an indication of at least the excitation energy of one of the possible perturbers (*vide infra*), and have therefore tested the above concept of interference by simulating two-photon excitation spectra of a $^2\Phi\leftarrow\leftarrow{}^2\Pi$ transition in the presence of an interaction with a state with different electronic symmetry.

The observed $^2\Phi$ Rydberg state is just one of the six Rydberg states ($^2\Delta$, $^2\Pi$, $^2\Phi$, $^2\Sigma^+$, $^2\Sigma^-$, and $^2\Gamma$) resulting from the configuration $[a\ ^1\Delta]3d\lambda$. The **L**-uncoupling operator, $-1/(2\mu R^2)(J^+L^- - J^-L^+)$, is known to mix Rydberg states which belong to the same l complex and differ by $\Delta\Lambda=\pm1$. Since the $^2\Gamma$ state is not accessible by two-photon absorption from the $^2\Pi$ ground state, we would expect *a priori* that the direct interaction with a $^2\Delta$ state would be dominant, and that such an interaction would to a major extent account for our observations. If l uncoupling between the identified $[a\ ^1\Delta]3d\pi\ ^2\Phi$ and the unknown $[a\ ^1\Delta]3d\sigma\ ^2\Delta$ state, placed $\sim$1600 cm^{-1} higher in energy (*vide infra*) with the same rotational parameters as the $^2\Phi$ state is assumed, qualitatively correct results are indeed obtained for the rotational branches which originate from the $F_1(^2\Pi_{3/2})$ component of the ground state: the intensity of the Q and S branches increases and decreases, respectively, while at the same time the higher members of the latter branch rapidly lose intensity. Furthermore, such an interaction causes an increase of the intensity of the ${}^sR_{21}$ branch in SD. We note that this simulation also predicts intensity changes for the branches originating from the $F_2(^2\Pi_{1/2})$ component of the ground state: here the R_2 and S_2 branches should decrease in intensity, whereas the intensity of the P_2 branch should increase. Since the experimental spectra do not allow, however, for definite statements on the intensity changes of these branches, confirmation of the influence of l uncoupling from these branches is not possible. An analysis of a more quantitative nature was impossible, since only the excitation energy of the perturber is known approximately and not its rotational parameters.

Evidence for the presence of a state with an excitation energy $\sim$1600 cm^{-1} higher than that of the $[a\ ^1\Delta]3d\pi\ ^2\Phi$ Rydberg state has been obtained with electron and mass-resolved ion detection for both the SH and SD radicals. At a one-photon energy of 39 817 cm^{-1} a very weak and fragmentary structure could be observed in the $(2+1)$ excitation spectrum of SD. Photoelectron spectra obtained at these excitation energies showed peaks deriving from ionization to both the vibrationless levels of the ground $X\ ^3\Sigma^-$ ionic state and the excited $a\ ^1\Delta$ ionic state. For SH two close-lying fragmentary structures were seen with mass-resolved ion detection. Employing electron detection these structures could be distinguished from each other by simultaneously monitoring photoelectrons with different kinetic energies. The photoelectrons for the lower-lying structure appeared to derive from an ionization process in which the SH^+ ion is left in its ground ionic state, while the other structure at slightly higher excitation energies ($\sim$40 cm^{-1}), derived from a state with the excited $[a\ ^1\Delta]$ ionic core. The former structure most probably corresponds to the $[X\ ^3\Sigma^-]5d\delta G\ ^2\Delta$ state seen in a VUV absorption study,[22] while the latter structure might be the $[a\ ^1\Delta]3d\sigma\ ^2\Delta$ Rydberg state. Assignment of the latter structure to another Λ component of the $[a\ ^1\Delta]3d\lambda$ complex is less likely (see Secs. III B and III C). The low intensity of this presumed $[a\ ^1\Delta]3d\sigma\ ^2\Delta$ Rydberg state in the $(2+1)$ REMPI spectrum of the SH and SD radicals makes it questionable that its two-photon transition moment is comparable to that to the $^2\Phi$ Rydberg state. The observed weak and fragmentary structures, though, could be due to a short-lived predissociative nature of the excited $[a\ ^1\Delta]3d\sigma\ ^2\Delta$ state caused by substantial Rydberg ($[a\ ^1\Delta]3d\sigma$) - valence ($[a\ ^1\Delta]6\sigma^*$) configuration mixing.

Notwithstanding that the observed intensity anomalies in the rotational branches of the $[a\ ^1\Delta]3d\pi\ ^2\Phi$ state can largely be accounted for by an l-uncoupling interaction with a higher-lying $[a\ ^1\Delta]3d\sigma\ ^2\Delta$ state, the negative value for the spin–orbit parameter A (see Table II) cannot be explained by such a mechanism. The required reversal in the Ω sequence in the $^2\Phi$ state can only derive from a homogeneous interaction between states with different electronic symmetries, such as spin–orbit interaction, because these interactions affect only one of the two Ω components. The $[a\ ^1\Delta]3d\sigma\ ^2\Delta$ state is not a likely candidate for such a process. First, a spin–orbit interaction between two Rydberg states belonging to the $[a\ ^2\Delta]3d\lambda$ configuration is expected to be negligible, since the off-diagonal spin–orbit matrix element will scale with the Rydberg A parameter which is

expected to be small. Second, if the spin–orbit interaction with a $^2\Delta$ state would be important, the perturbing $^2\Delta$ state would be required to have a lower vertical excitation energy than the $^2\Phi$ state in order to reverse the two Ω levels in this state. The $[a\ ^1\Delta]6\sigma^*\ ^2\Delta$ valence state, located below the $^2\Phi$ state, on the other hand, would be better suited as a perturber. This raises of course immediately the question whether the spin–orbit interaction between the $^2\Phi$ Rydberg state and $[a\ ^1\Delta]6\sigma^*\ ^2\Delta$ valence state might also account for the observed rotational intensity anomalies in the SH and SD spectra of the $^2\Phi$ state. Indeed, it is found from simulations that the characteristics of the experimentally observed intensity distribution are qualitatively well reproduced when we assume that the $^2\Phi$ state is coupled to a lower-lying $^2\Delta$ state by spin–orbit interaction. The principal difference between these simulations and those based upon l uncoupling is found in the intensity distributions over the F_2 branches. With l uncoupling (*vide supra*) the intensity of the R_2 and S_2 branches decreases and the intensity of the P_2 branch increases, whereas spin–orbit coupling results in the opposite behavior, i.e., R_2 and S_2 increase and P_2 decreases. Excitation spectra with even higher signal to noise ratios than the present ones might enable a detailed unraveling of the relative importance of the two coupling mechanisms.

The photoionization dynamics via the $[a\ ^1\Delta]3d\pi\ ^2\Phi$ state have been thoroughly investigated in two separate papers by rotationally resolved REMPI-PES and high-quality *ab initio* calculations[35,50] and will therefore only briefly be reviewed here. Rotationally resolved photoelectron spectra obtained after excitation of this state showed two particular characteristics of its photoionization dynamics, which were excellently reproduced by *ab initio* calculations. First, only transitions up to $\Delta N=\pm 2$ were observed, whereas transitions up to $\Delta N=\pm 4$ were expected. Second, strong asymmetries were observed in the ionic rotational branching ratios. The results of a recent ZEKE-PFI experiment on the $a\ ^1\Delta$ ionic state[14] in which the $[a\ ^1\Delta]3d\pi\ ^2\Phi$ state was used as an initial state for pulsed field ionization revealed the same characteristics as seen with direct ionization. A detailed comparison between the rotational branching ratios resulting from a pulsed-field ionization process and those of a direct ionization process has made it possible to elucidate the intrinsic details of the dynamical properties of the high-n Rydberg states involved in these ZEKE experiments.

In this section we identified the $[a\ ^1\Delta]3d\pi\ ^2\Phi\ (v'=0)$ state of the SH and SD radicals. Our assignment was based upon the small isotope shift in going from SH [Fig. 2(a)] to SD [Fig. 2(c)], the knowledge of the ionic core associated with these resonances (Fig. 3), energy considerations, and rotational analyses of the two-photon excitation spectra. From the observed line positions of the rotational transitions spectral parameters for this $^2\Phi$ state could be determined (Table II). The experimentally observed line intensities and the negative value derived for A suggest that several interactions such as l uncoupling and spin–orbit interaction determine the finer details of the spectroscopy of this state.

B. Excitation spectra between 80 100 and 80 750 cm^{-1}

Figure 4(a) shows the two-photon excitation spectrum of SD in the energy range of 80 100–80 750 cm^{-1} obtained using linearly polarized radiation and by monitoring only photoelectrons with a kinetic energy of about 3.3 eV. This photoelectron energy corresponds to ionization of the molecule into the $a\ ^1\Delta$ ionization continua. The excitation spectrum is very weak and shows only sparse rotational structure. When the polarization of the excitation light is changed from linear to circular, some of the rotational branches increase in intensity, while at the same time at least one branch disappears [Fig. 4(b)]. Moreover, in contrast to other observed two-photon excitation spectra of Rydberg states of SD, both excitation spectra show a remarkably low intensity for the transitions from the F_2 ($^2\Pi_{1/2}$) component of the electronic ground state. Attempts to detect REMPI transitions for the SH radical in this region were not successful.

Figure 5 depicts the photoelectron spectrum obtained via the R_1 rotational bandhead at a one-photon energy of 40 311 cm^{-1}. The small photoelectron peak with a kinetic energy of about 3.3 eV derives from a (2+1) ionization process in which the ground state $X\ ^2\Pi\ (v''=0)$ SD radical is ionized into the vibrationless $a\ ^1\Delta$ ionization continua of the SD^+ ion. The remaining two photoelectron peaks of larger intensity can be attributed to a (2+1) ionization process of the parent D_2S: the $^1A_1$ ground state is ionized into the $v_1^+=0$ and $v_1^+=1$ continua of the $X\ ^2B_1$ ground ionic state via the nearby two-photon resonance at 80 820 cm^{-1} identified before as the $^1B_1\ (2b_1)^1(7pa_1)^1$ Rydberg state.[51] We can consequently conclude that the observed Rydberg state is built upon the excited $a\ ^1\Delta\ (v^+=0)$ ionic state.

The dependence of the two-photon excitation spectra on the polarization of the excitation light would seem to indicate that the sparse rotational structure in Figs. 4(a) and 4(b) should be attributed to a two-photon $^2\Pi\leftarrow\leftarrow{}^2\Pi$ transition. Such a transition may in principle derive its intensity from three components of the two-photon transition tensor: the totally symmetric zero-rank component T_0^0, which allows for $\Delta J=0$ transitions, and the $T_{\pm 2}^2$ and T_0^2 components, which are associated with $\Delta J=0,\pm 1,\pm 2$ rotational transitions. Changing the polarization of the excitation light from linear to circular results in the disappearance of all contributions carried by the T_0^0 transition tensor, while those carried by the $T_{\pm 2}^2$ and T_0^2 components are expected to increase by a factor of 1.5. Our observation that at least one rotational branch all but disappears when circularly polarized excitation light is employed, implies that the transition derives from the T_0^0 component and, consequently, that the excited state is of $^2\Pi$ symmetry. On the basis of the quantum defect ($\delta=0.15$) derived from the excitation energy, and the knowledge of the ionic core associated with this resonance, the observed $^2\Pi$ Rydberg state should have the same configuration as the $[a\ ^1\Delta]3d\pi\ ^2\Phi$ state discussed previously. The two-photon transition to this $[a\ ^1\Delta]3d\pi\ ^2\Pi$ state, though formally forbidden in an ''atomiclike'' picture can obtain some transition

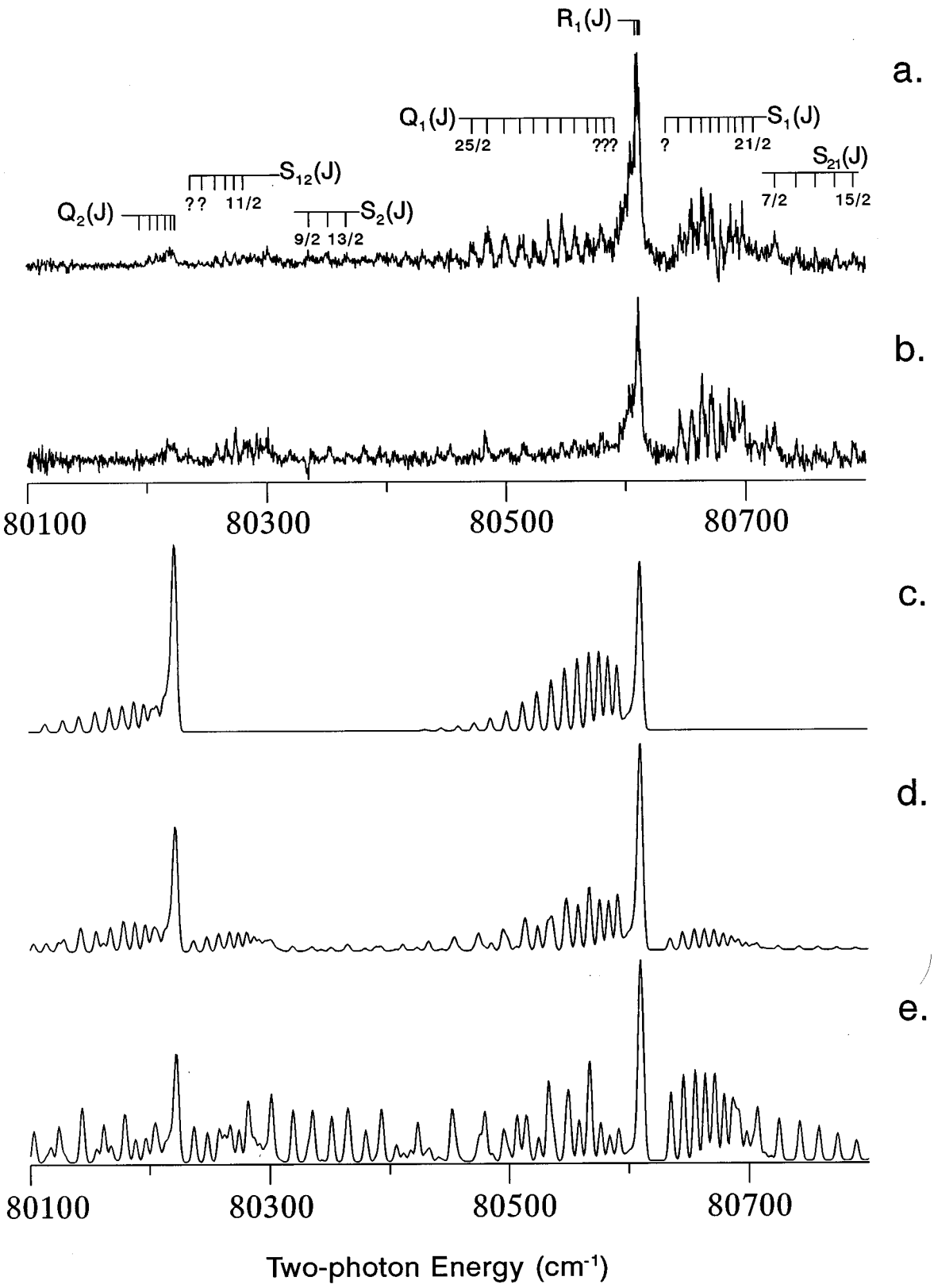

FIG. 4. (a) Two-photon excitation spectrum of the $[a\ ^1\Delta]3d\pi\ ''^2\Pi''\ (v'=0)\leftarrow\leftarrow X\ ^2\Pi\ (v''=0)$ transition in SD using linearly polarized excitation light. Individual line assignments are given by the combs above the spectrum. The question marks indicate the excitation wavelengths at which transitions to the $N'=1$, 2, and 3 levels would have been expected (see the text for further details). (b) Two-photon excitation spectrum of the $[a\ ^1\Delta]3d\pi\ ''^2\Pi''\ (v'=0)\leftarrow\leftarrow X\ ^2\Pi\ (v''=0)$ transition in SD using circularly polarized excitation light. (c) Simulated excitation spectrum showing the contribution of the T_0^0 zero-rank component. The spectrum has been calculated using the spectroscopic constants given in Table II and a Gaussian linewidth of 4 cm^{-1}. (d) Simulated excitation spectrum showing the contribution of the $T_{\pm 2}^2$ tensor component. (e) Simulated excitation spectrum showing the contribution of the T_0^2 tensor component. Spectra (a) and (b) were obtained with electron detection.

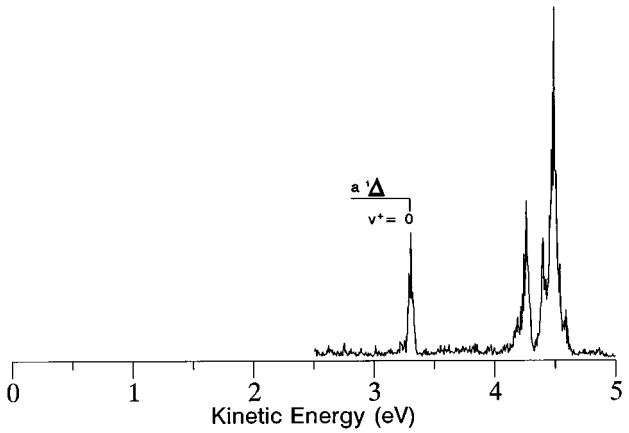

FIG. 5. Photoelectron spectrum obtained for (2+1) ionization via the R_1 rotational bandhead of the transition to the $[a\ ^1\Delta]3d\pi\ ^{\prime\prime}\ ^2\Pi^{\prime\prime}$ ($v'=0$) state of SD. The peaks not marked in the figure derive from ionization of the parent D_2S molecule (see the text for further details).

probability for the same reason as suggested for the $[a\ ^1\Delta]3d\pi\ ^2\Phi$ state (*vide supra*).

Rotational analyses of the excitation spectra shown in Figs. 4(a) and 4(b) have enabled us to identify all observed lines, while a least-squares fit to the line positions resulted in the spectral parameters given in Table II. Figures 4(c)–4(e) show the contributions of the various tensor components based upon these constants. In Fig. 4(c) it is assumed that the excitation is only carried by the totally symmetric zero-rank component T_0^0, while in Figs. 4(d) and 4(e) the contributions from the $T_{\pm 2}^2$ and T_0^2 tensor components are shown. Despite the fact that the polarization dependence seems to allow an unambiguous symmetry assignment for this Rydberg state, and despite the reasonably good least-squares fit to the observed line positions (Table II), all attempts failed to simulate even qualitatively the intensities of the rotational transitions in the linearly and circularly polarized excitation spectra by taking squares of various sums over the relevant components of the two-photon transition tensor. The most striking discrepancy in this respect is that the circularly polarized two-photon excitation spectrum of Fig. 4(b) is dominated by R_1 and S_1 rotational branches, whereas the $T_{\pm 2}^2$ and T_0^2 [see Figs. 4(d) and 4(e)] second-rank tensor components also carry significant line strength for all other rotational branches.

A second difference between experiment and theory concerns the aforementioned low intensities of the rotational transitions originating from the $F_2(^2\Pi_{1/2})$ component of the electronic ground state. It might be argued that the overall population in the ground $^2\Pi_{3/2}$ and the $^2\Pi_{1/2}$ spin–orbit states of SD could differ from the expected 3:2 ratio. This seems, however, very unlikely, since for all other measured energy regions a ratio of about 3:2 is found to be adequate.

A third difference between the experimental and theoretical spectra, which is observed irrespective of the laser polarization, is that all transitions to the $N'=1$, 2, and 3 levels are missing. This is illustrated by the question marks in Fig. 4(b), which indicate where such transitions should occur. One could therefore question the validity of the symmetry assignment for the observed two-photon resonant Rydberg state, since only for an excited state with Γ symmetry are such transitions expected to be absent. Such a conclusion would seem, however, to be in conflict with the observed dependence on the polarization of the laser radiation, and last but not least, in conflict with the fact that a $^2\Gamma\leftarrow\leftarrow{}^2\Pi$ two-photon transition violates the two-photon selection rule $\Delta\Lambda=0,\pm 1,\pm 2$. For the moment we shall therefore try to explain the observed intensity anomalies under the assumption that the excited state is indeed of $^2\Pi$ symmetry.

For the $[a\ ^1\Delta]3d\pi\ ^2\Phi$ state *l* uncoupling, resulting in an interaction with the $[a\ ^1\Delta]3d\sigma\ ^2\Delta$ state, and/or spin–orbit coupling with the $[a\ ^1\Delta]6\sigma^*$ valence state, was shown to be able to account for the observed intensity distribution over the rotational branches. Both mechanisms have been investigated here also and it was found that an *l*-uncoupling interaction between the $[a\ ^1\Delta]3d\pi\ ^2\Pi$ state and the $[a\ ^1\Delta]3d\sigma\ ^2\Delta$ state could be responsible for the intensity anomalies observed in the two-photon excitation spectra. We have investigated the effects of *l* uncoupling by simulating circularly polarized excitation spectra of a $^2\Pi\leftarrow\leftarrow{}^2\Pi$ transition under the assumption of a relatively strong interaction with the same $^2\Delta$ perturber located at 9.87 eV. In these simulations it was assumed that the two-photon transition to the unperturbed $^2\Pi$ state was carried by the $T_{\pm 2}^2$ transition tensor component. These simulations demonstrate that qualitatively reasonable agreement could be obtained between experiment and theory: the low frequency end of the calculated $^2\Pi\leftarrow\leftarrow{}^2\Pi$ spectrum shows an overall reduced intensity for the rotational lines from the F_2 ($^2\Pi_{1/2}$) component of the ground state, while at the same time the R_1 and S_1 rotational branches, originating from the F_1 ($^2\Pi_{3/2}$) component, tend to dominate the high frequency end of the spectrum. No quantitative agreement with the experimental spectrum of Fig. 4(b) could be achieved, because of the crude assumptions about the rotational parameters of the $^2\Delta$ state (*vide supra*), and because of the unknown contribution of the T_0^2 component. Note in this respect also that only one perturber was assumed, whereas in a complete *l*-uncoupling treatment one would have to take *l* mixing with other states, most notably $^2\Sigma^{\pm}$ states, into account as well.

It is doubtful whether the absence of all transitions to the lowest three rotational levels in the excited $^2\Pi$ state can be explained by the interaction(s) proposed above. The simulations, in which *l* uncoupling was incorporated, indicate a mere intensity decrease for these transitions, but never show a complete disappearance. The absence of a few lines is usually indicative of the presence of a very localized interaction in which the perturbed and perturbing states have similar energies. In that respect the difference in excitation energy for the $^2\Pi$ and $^2\Delta$ states, $\sim$800 cm^{-1}, is too large to account for a local perturbation at low N' values.

The disappearance of a few lines might be explained by a localized predissociation mechanism. *Ab initio* calculations suggest that the states deriving from a $5\sigma\rightarrow 6\sigma^*$ excitation, [$^4\Pi$, $^2\Pi$ $(2x)$], have vertical excitation energies just within

the Rydberg region involving the various $^4\Pi$, $^2\Pi$, and $^2\Phi$ states related to the configurations $5\sigma^2 2\pi^2 4p\pi$ and $5\sigma^2 2\pi^2 3d\pi$. The lowest $^2\Pi$ state of this $5\sigma^1 2\pi^3 6\sigma^{*1}$ family can be regarded as a possible candidate to induce electrostatic predissociation of the SD $[a\ ^1\Delta]3d\pi\ ^2\Pi$ $(v'=0)$ level, since it acquires a purely repulsive character for bond lengths larger than the ground state equilibrium distance. Such an explanation would be consistent with our inability to detect the equivalent transition in the SH spectrum. One might object that such a homogeneous predissociation mechanism is not dependent on J. A J dependence can, however, derive from vibration–rotation interaction,[52] which could influence the vibrational overlap in the interaction matrix element. This might thus lead to an *a priori* unexpected localization for homogeneous predissociation.

When the parameters (Table II) obtained from the rotational analysis of the excitation spectrum are compared with those of the excited $a\ ^1\Delta$ ionic state (Table I), we note that the $^2\Pi$ state has a rotational constant B_0, which is considerably smaller than that of the $a\ ^1\Delta$ ionic state. Moreover, an unexpected negative value for the centrifugal distortion parameter D_0 is derived. Although the negative D_0 value can also be accounted for by l uncoupling with a $^2\Delta$ state with a lower excitation energy than the $^2\Pi$ state, these data, and the failure to observe the equivalent transition in SH, strongly suggest that valence-Rydberg mixing is important, irrespective of the question whether it might be able to explain the absence of the $N'=1$, 2, and 3 levels in the $^2\Pi$ state.

Several other mechanisms can be put forward as well. A local perturbation, either homogeneous or heterogeneous in character, might result in a simple intensity transfer if the perturbation would involve a ''bright'' $^2\Pi$ state and a very nearby ''dark'' background state of $^2\Sigma$, $^2\Pi$, or $^2\Delta$ symmetry. However, such a local perturbation between bound states is generally accompanied by the appearance of extra lines in the excitation spectrum. It is also possible that interference of two identical two-photon transition moments of comparable strengths results in the disappearance of a few lines.[53] Such an interference can arise from the interaction between two bright states of the same electronic symmetry and can cause a transfer of intensity in such a way that *all* ΔJ rotational transitions to a particular upper J are affected in exactly the same fashion.[48,49,53] However, until now no evidence for a nearby second bright $^2\Pi$ state has been found, while the $^2\Pi$ states which will be discussed in Sec. III D, have too high an excitation energy to play a role. A last possibility concerns predissociation of isolated rotational levels due to a three-state interaction involving a local perturbation by a weakly predissociated level (accidental predissociation).[54] Whatever the nature of the local perturbation, we should also observe deviations from the regular line positions of other ''unperturbed'' N' levels. Our results are peculiar in that respect, since all transitions to $N'=1$, 2 and 3 are missing, whereas no energy level shifts could be detected for $N'=4$ and higher rotational levels. This sheds considerable doubt on an explanation in terms of a local perturbation.

All these considerations lead one to return to the $^2\Gamma$ symmetry assignment discarded previously. Formally a $^2\Gamma \leftarrow\leftarrow {}^2\Pi$ two-photon transition violates selection rules, but it might borrow part of its intensity from an excited $^2\Pi$ state. The attraction of this explanation would be that the absence of transitions to excited states levels with $N'\leqslant 3$ and the observed polarization dependence behavior arise naturally. A drawback is that one needs at least a three-step interaction mechanism, such as a three-step indirect l-uncoupling perturbation, to mix the $[a\ ^1\Delta]3d\pi\ ^2\Pi$ state with the $[a\ ^1\Delta]3d\delta\ ^2\Gamma$ state.

In conclusion, we have identified a previously unobserved Rydberg state of which we know with certainty that it has a $[a\ ^1\Delta]3d$ configuration based on the determination of its ionic core from photoelectron spectra and the quantum defect derived from its excitation energy. Moreover, from the observed resonance positions of the rotational transitions the spectral parameters of this $[a\ ^1\Delta]3d$ state could be determined. A more definite assignment of the exact symmetry of this state is hampered by a number of conflicting observations. The observed polarization dependence of the excitation spectra would seem to indicate that we deal with the $[a\ ^1\Delta]3d\pi\ ^2\Pi$ Rydberg state. In that case we cannot account very satisfactorily for the absence of the $N'=1$, 2, and 3 levels and the unperturbed character of higher levels. If a $[a\ ^1\Delta]3d\delta\ ^2\Gamma$ Rydberg state is assumed, the absence of transitions to the $N'=1$, 2 and 3 levels comes out in a straightforward manner, but then a complicated interaction mechanism with a $^2\Pi$ state would be required to explain the intensity of this ''forbidden'' transition and its polarization dependence.

C. Excitation spectra between 81 100 and 82 750 cm^{-1}

Figure 6(a) displays the two-photon excitation spectrum of SH in the two-photon energy region between 81 200 and 82 200 cm^{-1}, obtained by monitoring only photoelectrons with a kinetic energy of about 2.5 eV. They derive from a (2+1) photoionization process in which the SH^+ ion is created in its second excited state, $b\ ^1\Sigma^+$. The rotational analysis of this spectrum allows for the conclusion that the resonance enhancing state is of $^2\Sigma$ symmetry, as evidenced, for example, by the observation of transitions from both the $^2\Pi_{1/2}$ and $^2\Pi_{3/2}$ ground state spin–orbit components to excited state levels with $J'=1/2$. The analysis has enabled us to identify most of the observed lines. A least-squares fit to the line positions resulted in the spectral parameters given in Table II.

The analogous two-photon spectrum for the SD isotope was observed at slightly higher excitation energies and is depicted in Fig. 6(c). Although this spectrum also shows rotational resolution, its analysis was considerably more difficult and not as unambiguous as for the previous excitation spectrum. The validity of the spectral parameters obtained for this state, presented in Table II, must consequently be taken with some caution.

Figures 7(a) and 7(b) display typical photoelectron spectra for the (2+1) ionization process via the newly observed $^2\Sigma$ state of SH and SD, respectively. The dominant photo-

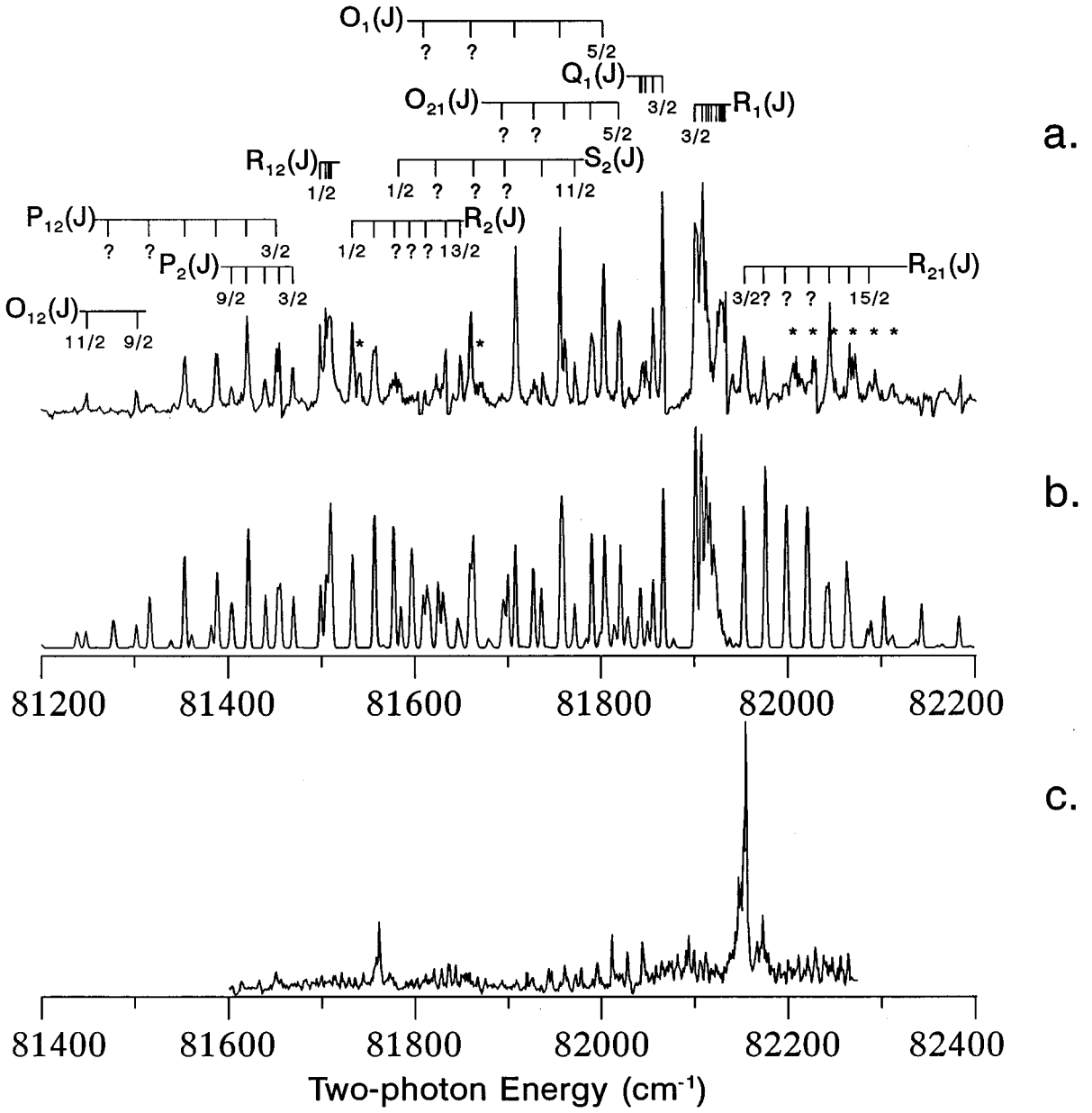

FIG. 6. (a) Experimental two-photon excitation spectrum of the $[b\ ^1\Sigma^+]4p\sigma\ ^2\Sigma^+\ (v'=0)\leftarrow\leftarrow X^2\Pi\ (v''=0)$ transition in SH. Individual line assignments are given by the combs above the spectrum. The question marks indicate the excitation wavelengths at which transitions to the $N'=4$, 5, and 6 levels would have been expected. In the experimental spectrum these are either absent or have an intensity which is lower than what simulations would predict. The transitions marked with an asterisk derive from excitation of another excited state, whose identity is not known (see the text for further details). (b) Simulated spectrum for SH using the spectroscopic constants given in Table II and a Gaussian linewidth of 3 cm^{-1}. (c) Experimental two-photon excitation spectrum of the $[b\ ^1\Sigma^+]4p\sigma\ ^2\Sigma^+\ (v'=0)\leftarrow\leftarrow X\ ^2\Pi\ (v''=0)$ transition in SD. Spectra (a) and (c) were obtained with electron detection.

electron peak in these spectra originates from photoionization of the ground state $X\ ^2\Pi\ (v''=0)$ of SH (SD) by absorption of three photons into the third electronic vibrationless ionization continua of the SH^+ (SD^+) ion. We can therefore conclude that the observed Rydberg state is principally built upon the excited $b\ ^1\Sigma^+\ (v^+=0)$ ionic state. The measured quantum defects, 1.71 and 1.70 with $n=4$ for SH and SD, respectively, indicate that the Rydberg electron has $4p$ character. In the first instance the observed $^2\Sigma$ state should, consequently, be associated with the $[b\ ^1\Sigma^+]4p\sigma$ configuration. From Figs. 7(a) and 7(b) we derive a value for the third electronic ionization energy of the SH and SD radicals of 12.74 ± 0.01 and 12.73 ± 0.01 eV, respectively. The value for SH agrees reasonably well with the previous determination of 12.76 eV from HeI VUV PES measurements.[12] Figures 7(a) and 7(b) show, apart from the photoelectrons with a kinetic energy of 2.5 eV, weaker peaks whose kinetic energies are consistent with ionization into the first excited $(v^+=1)$ vibrational level of the same $b\ ^1\Sigma^+$ ionic state, and with the formation of the first three $(v^+=0, 1, 2)$ vibrational levels of the lower-lying excited $a\ ^1\Delta$ ionic state. When the intensities of these weaker photoelectron peaks are moni-

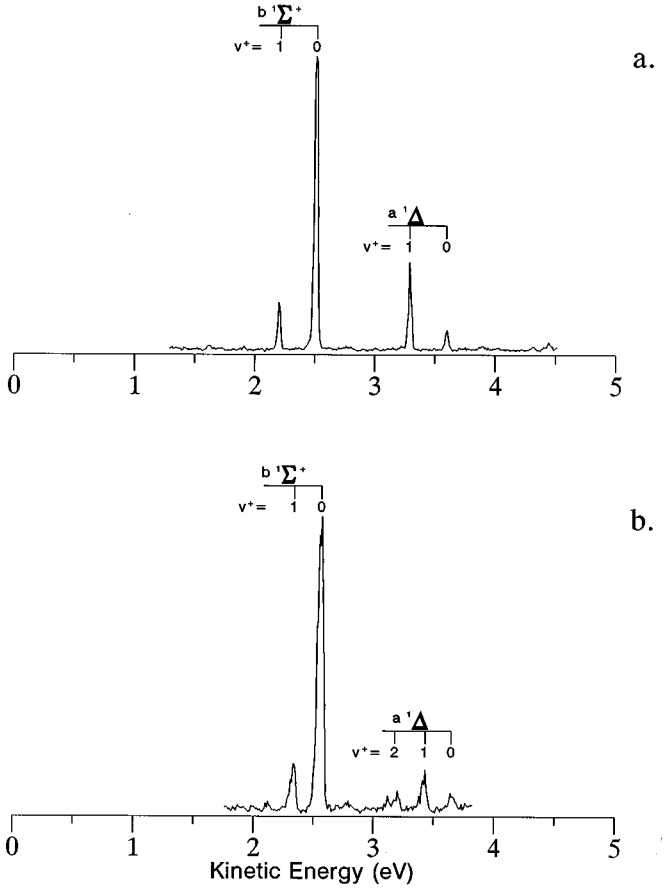

FIG. 7. Photoelectron spectra obtained for (2+1) ionization via the $[b\ ^1\Sigma^+]4p\sigma\ ^2\Sigma^+$ ($v'=0$) state of (a) SH, taken at a one-photon energy of 40 908 cm^{-1}, (b) SD, taken at a one-photon energy of 40 887 cm^{-1}.

tored as a function of excitation wavelength, excitation spectra are obtained which are practically the same as those depicted in Figs. 6(a) and 6(c). Table III summarizes the spectroscopic level spacings for the $a\ ^1\Delta$ and $b\ ^1\Sigma^+$ states of the SH^+ and the SD^+ ions, as derived from an analysis of all recorded REMPI-PES spectra (see also below). The values for the separation between the first two vibrational levels of the $a\ ^1\Delta$ and $b\ ^1\Sigma^+$ SH^+ ionic states, 307 and 306 meV, respectively, match previously obtained values[12] very well.

TABLE III. Vibrational level spacings (cm^{-1}) for the $a\ ^1\Delta$ and $b\ ^1\Sigma^+$ excited states of SH^+ and SD^+ as measured by REMPI-PES, together with derived vibrational constants. The uncertainty in the measured spacings is 40 cm^{-1}.

	Ionic states	$a\ ^1\Delta$	$b\ ^1\Sigma^+$
SH^+	$\nu_1-\nu_0$	2479	2469
	$\nu_2-\nu_1$	2367	2374
	$\nu_3-\nu_2$	2297	
SD^+	$\nu_1-\nu_0$	1784	1838
	$\nu_2-\nu_1$	1818	1758
	$\nu_3-\nu_2$	1501	
SH^+	ω_e	2556	2563
	$\omega_e x_e$	45	47
SD^+	ω_e	2042	1918
	$\omega_e x_e$	71	40

In the single-configuration approximation of a Rydberg state a Rydberg electron is loosely bound to one specific state of the ion. For the photoionization of such a state one expects that the ionic configuration remains unchanged. As the potential energy surfaces of the Rydberg state and its associated ionic state have in general the same shape and equilibrium distance, Franck–Condon considerations would favor almost exclusively ionization with conservation of the vibrational quantum number. For the $^2\Sigma^+$ state investigated here we see for the final photoionization step (Fig. 7) a deviation from this $\Delta v=0$ propensity rule and, most important, a deviation from the expected ionic core preservation. We must therefore conclude that the present $^2\Sigma^+$ state is significantly perturbed as a result of which its appropriate description requires not only the $[b\ ^1\Sigma^+]4p\sigma$ configuration, but configuration(s) based on the $a\ ^1\Delta$ ionic core as well. The difference in excitation energies (240 cm^{-1}) between the SH and the SD isotopes (see Table II) is consistent with the perturbation suggested above, since this shift is significantly larger than the negligible isotope shifts seen before for $v'=0\leftarrow v''=0$ transitions, but too small to be ascribed to differences in vibrational quantum numbers.

A closer analysis of the excitation spectrum of the SH radical provides additional indications for perturbation(s). Figure 6(b) displays the simulated spectrum of a $^2\Sigma^+\leftarrow\leftarrow{}^2\Pi$ transition using the constants derived from the rotational analysis. Despite the reasonable least-squares fit of most of the rotational lines in Fig. 6(a), the simulated and experimental spectra differ in some aspects. The most striking difference is that the experimental spectrum reveals a sudden drop in intensity in *all* rotational branches for rotational transitions involving the final upper state levels $N'=4$, 5, and 6, and that the intensity reappears for higher N' values. This discrepancy between experimental [Fig. 6(a)] and simulated [Fig. 6(b)] spectra is illustrated by question marks in Fig. 6(a), which indicate the excitation energies for some of these rotational transitions. One might question the employed ground state rotational distribution of 300 K over each spin–orbit component. However, for all other energy regions, higher as well as lower, an approximate Boltzmann rotational distribution of 300 K was found to be adequate.

An anomalously low intensity of *all* transitions involving particular rotational levels is usually an indication for the presence of a very localized interaction in which the perturbed and perturbing states have similar energies. Further experimental evidence for the presence of a localized perturbation is found in the differences between the observed and calculated line positions, especially those that involve the upper state levels around $N'=5$. Moreover, in the experimental spectrum [Fig. 6(a)], some weak and diffuse lines are present which do not have counterparts in the simulated spectrum [Fig. 6(b)]. These lines are marked with asterisks in Fig. 6(a). In Sec. III B various possibilities for local perturbations were discussed. One of them concerned the interaction between a ''bright'' and a very nearby ''dark'' back-

ground state. The appearance of the extra lines in Fig. 6(a) could therefore involve rotational transitions to an unknown dark state which borrows transition probability from our identified bright $^2\Sigma^+$ state.

Despite the fact that the extra lines appear to form a S_1 or $^sR_{21}$ rotational branch at the higher energy part of the excitation spectrum [Fig. 6(a)] the total number of extra lines was not sufficient to allow for a rotational analysis. Note that normally with REMPI-PES one would obtain additional information on the character of the local perturber by comparison of the photoelectron spectra associated with the main and extra lines. We hardly see any significant differences, probably due to the close vicinity of the line positions of the main and extra transitions. Presently, we cannot decide about the homogeneous or heterogeneous character of the local interaction. Experimental observations to be discussed below will show, however, that this perturbation is not responsible for the deviations from the expected ionic core conservation in the photoelectron spectra of the $[b\ ^1\Sigma^+]4p\sigma\ ^2\Sigma^+$ excited state (Fig. 7).

Inspection of the photoelectron spectra shown in Fig. 7 reveals that the (2+1) REMPI process yields SH^+ (SD^+) ions predominantly in the vibrationless level of the $b\ ^1\Sigma^+$ ionic state, in agreement with the dominant $[b\ ^1\Sigma^+]4p\sigma\ ^2\Sigma^+$ ($v'=0$) composition, but also with a considerable probability in the $a\ ^1\Delta$ ($v^+=1$) level. This latter photoionization probability indicates that the vibronic character of the perturber is a Rydberg state built upon the $a\ ^1\Delta$ ionic core in its first excited vibrational level. Energy considerations would suggest $3d$ character for the Rydberg electron. In the single-configuration approximation the configurations of the $[b\ ^1\Sigma^+]4p\sigma$ state and an $[a\ ^1\Delta]3d\lambda$ state differ by two spin–orbitals, i.e., the Rydberg orbital and one of the core spin orbitals. Only the two-electron operator $\Sigma e^2/r_{ij}$, which is part of the electronic Hamiltonian, has a nonzero off-diagonal matrix element between the two considered configurations. Since electrostatic perturbation only occurs between states of identical symmetry we conclude that the perturbing state is the $[a\ ^1\Delta]3d\delta\ ^2\Sigma^+$ ($v'=1$) state.

The presence of the $[a\ ^1\Delta]3d\delta\ ^2\Sigma^+$ ($v'=1$) perturber has been verified by additional experiments. Figure 8(a) shows the two-photon excitation spectrum of SD in the two-photon energy region between 81 100 and 81 750 cm^{-1} obtained by monitoring photoelectrons with a kinetic energy of about 3.3 eV. This kinetic energy corresponds to a (2+1) photoionization process, in which SD^+ is left in the $v^+=1$ level of the $a\ ^1\Delta$ excited state. Rotational analysis of this excitation spectrum reveals it to be associated with a $^2\Sigma\leftrightarrow{}^2\Pi$ transition. The spectroscopic parameters derived from the fit of the observed rotational transitions are listed in Table II, while the simulated spectrum based upon these constants is depicted in Fig. 8(b). In the case of SH a weak and fragmentary structure can be observed ~800 cm^{-1} higher in energy [Fig. 8(c)]. Rotational analysis is difficult, but assignment of, in particular, the members of an R_{21} branch, which are clearly present at the higher energy side of the excitation spectrum, enabled us to derive its rotational parameters (Table II). Figure 8(d) shows the simulated SH spectrum. From the observed difference in excitation energies between SH and SD (~800 cm^{-1}) it is clear that the transition to this particular $^2\Sigma^+$ state involves a change in vibrational quantum number. In fact, the difference of about 800 cm^{-1} is more or less what is expected for a transition from the $X\ ^2\Pi$ ($v''=0$) ground state to the $v'=1$ level of a Rydberg state whose vibrational frequency is similar to that of the $a\ ^1\Delta$ or $b\ ^1\Sigma^+$ ionic state (see Table III).

Figure 9(a) displays the SD photoelectron spectrum obtained for ionization via the R_{12} rotational bandhead at a one-photon energy of 40 637 cm^{-1}. The photoelectron spectrum of SH [Fig. 9(b)] has been measured via the strongest observed resonance at a one-photon energy of 41 255 cm^{-1}. The resemblance between the two spectra is clear: both show photoelectrons peaks deriving from a photoionization process in which the ground state $X\ ^2\Pi$ ($v''=0$) absorbs three photons and is ionized into both the second ($a\ ^1\Delta$) and third ($b\ ^1\Sigma^+$) electronic ionization continua. In each spectrum a major peak involves photoelectrons which correspond to the formation of ions in the $a\ ^1\Delta$ ($v^+=1$) level. Figure 9 is thus consistent with an assignment of the ionic core of this second $^2\Sigma^+$ state as $a\ ^1\Delta$ ($v^+=1$).

The excitation spectra shown in Fig. 8 and the accompanying photoelectron spectra depicted in Fig. 9 confirm the presence of the $[a\ ^1\Delta]3d\delta\ ^2\Sigma^+$ ($v'=1$) Rydberg state, which is considered to be the perturber of the $[b\ ^1\Sigma^+]4p\sigma\ ^2\Sigma^+$ ($v'=0$) Rydberg state. On the basis of the observed excitation energies in SH and SD, the $[a\ ^1\Delta]3d\delta\ ^2\Sigma^+$ ($v'=0$) state should be located at ~9.90 eV, in good agreement with the results of *ab initio* calculations.[24] As was shown in Sec. III A, the only observed origin in this energy region was located at ~9.87 eV, which was assigned to the $[a\ ^1\Delta]3d\sigma\ ^2\Delta$ state. In the first instance one might (re)assign this origin to the $[a\ ^1\Delta]3d\delta\ ^2\Sigma^+$ ($v'=0$) state, but this would imply that this state would have a vibrational frequency which would be more than 20% larger than the frequency of its ionic core. This seems highly unlikely, and we therefore conclude that the vibrationless transition to the $[a\ ^1\Delta]3d\delta\ ^2\Sigma^+$ state cannot be observed in our experiments.

Since the two identified $^2\Sigma^+$ states interact strongly, their appropriate wave functions should be described by a linear combination of the two configurations involved:

$$\begin{aligned} {}^2\Sigma^+(1) &= [b\ ^1\Sigma^+]4p\sigma\ ^2\Sigma^+(v'=0) \\ &\quad + H^{\mathrm{el}}/\Delta E[a\ ^1\Delta]3d\delta\ ^2\Sigma^+(v'=1), \\ {}^2\Sigma^+(2) &= [a\ ^1\Delta]3d\delta\ ^2\Sigma^+(v'=1) \\ &\quad + H^{\mathrm{el}}/\Delta E[b\ ^1\Sigma^+]4p\sigma\ ^2\Sigma^+(v'=0) \end{aligned} \tag{1}$$

with

$$\begin{aligned} H^{\mathrm{el}} &= \langle [a\ ^1\Delta]3d\delta\ ^2\Sigma^+ | \Sigma e^2/r_{ij} | [b\ ^1\Sigma^+]4p\sigma\ ^2\Sigma^+ \rangle \\ &\quad \times (v'=0 | v'=1) \end{aligned} \tag{2}$$

and ΔE the energy separation between the unperturbed states. Note, that the ordering of the $^2\Sigma^+(1)$ and $^2\Sigma^+(2)$ states is reversed for SD with respect to SH. In such a two-state

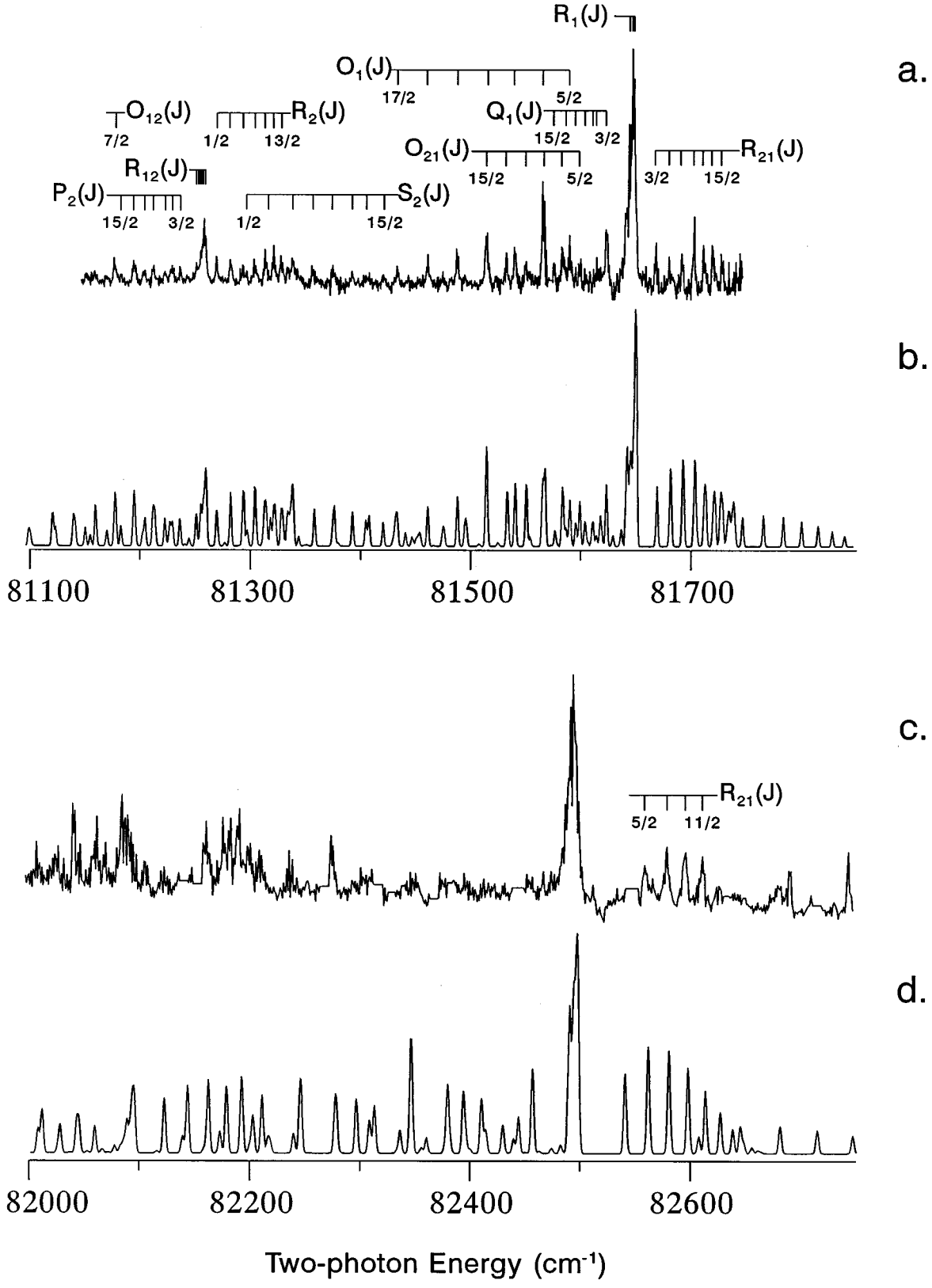

FIG. 8. (a) Experimental two-photon excitation spectrum of the $[a\ ^1\Delta]3d\delta\ ^2\Sigma^+\ (v'=1)\leftarrow\leftarrow X\ ^2\Pi\ (v''=0)$ transition in SD. Individual line assignments are given by the combs above the spectrum. (b) Simulated excitation spectrum for SD using the spectroscopic constants given in Table II and a Gaussian linewidth of 2 cm^{-1}. (c) Experimental two-photon excitation spectrum of the $[a\ ^1\Delta]3d\delta\ ^2\Sigma^+\ (v'=1)\leftarrow\leftarrow X\ ^2\Pi\ (v''=0)$ transition in SH. The straight horizontal lines derive from the removal of strong sulfur resonances at those positions. (d) Simulated excitation spectrum for SH using the spectroscopic constants given in Table II and a Gaussian linewidth of 3 cm^{-1}. Spectra (a) and (c) were obtained with electron detection.

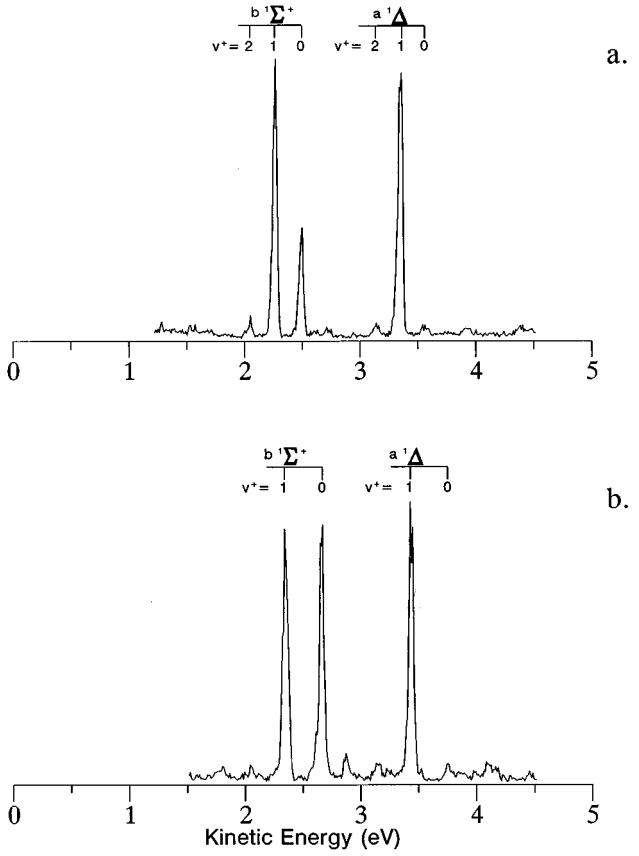

FIG. 9. Photoelectron spectra obtained for (2+1) ionization via the $[a\ ^1\Delta]3d\delta\ ^2\Sigma^+$ $(v'=1)$ state of (a) SD, taken at a one-photon energy of 40 637 cm^{-1}, (b) SH, taken at a one-photon energy of 41 255 cm^{-1}.

interaction model we expect that the REMPI-PES spectra via each $^2\Sigma^+$ state would roughly reflect the composition of the Rydberg state wave functions. Comparison of the REMPI-PES spectra obtained via the $^2\Sigma^+(1)$ (Fig. 7) and $^2\Sigma^+(2)$ (Fig. 9) states indeed shows that for the $^2\Sigma^+(2)$ state ionization occurs with a relative decrease in the formation of SH^+ (SD^+) ions in the $v^+=0$ level of the $b\ ^1\Sigma^+$ ionic state. At the same time an increase in the probability of forming ions in the $v^+=1$ level of the $a\ ^1\Delta$ ionic state is observed. A direct comparison between the branching ratios observed in the photoelectron spectra and the wave function composition is, however, not possible since the intensities in these spectra also depend on the relative photoionization cross sections to the two ionic cores. Our REMPI-PES spectra (Figs. 7 and 9) indicate a larger photoionization probability to the $b\ ^1\Sigma^+$ ionization continua, since the observed ionic ratio $a\ ^1\Delta$ $(v^+=1):b\ ^1\Sigma^+$ $(v^+=0)$ in Fig. 9 is much smaller than the $b\ ^1\Sigma^+$ $(v^+=0):a^1\Delta$ $(v^+=1)$ ionic ratio in Fig. 7.

Although the excitation and photoelectron spectra of the two $^2\Sigma^+$ states discussed here show unambiguous evidence for an interaction between the two states, we nevertheless must conclude that the two-state model is still an oversimplification. This becomes evident when we consider the following observations. First, the excitation energies and rotational parameters of the two states in SH show that the local perturbation around $N'=5$ in the $[b\ ^1\Sigma^+]4p\sigma\ ^2\Sigma^+$ $(v'=0)$ state which we had to assume, cannot be caused by the $[a\ ^1\Delta]3d\sigma\ ^2\Sigma^+$ $(v'=1)$ state, since a level crossing is only predicted for considerably higher values of N'. Second, with the two-state interaction model we would principally expect the formation of ions in the vibrationless level of the $b\ ^1\Sigma^+$ state and the $v^+=1$ level of the $a\ ^1\Delta$ ionic state. Minor deviations are not unusual, but the significant probability for making ions in the $v^+=1$ level of the $b\ ^1\Sigma^+$ state when photoionizing via the $[a\ ^1\Delta]3d\delta\ ^2\Sigma^+$ $(v'=1)$ state is certainly not expected. Finally, the off-diagonal matrix element H^{el} [Eq. (2)] includes the overlap of the vibrational wave functions $[v'=1([a\ ^1\Delta]3d\delta\ ^2\Sigma^+)|v'=0([b\ ^1\Sigma^+]4p\sigma\ ^2\Sigma^+)]$. Generally, the potential energy curve of a Rydberg state is quite similar to that of the ionic state upon which it converges. Experimentally and theoretically it has been shown that the potential energy curves of the $a\ ^1\Delta$ and $b\ ^1\Sigma^+$ ionic states of SH (SD) resemble each other to a large extent. This observation would imply that the vibrational overlap would be very small, and would consequently lead to the conclusion that the interaction between $[b\ ^1\Sigma^+]4p\sigma\ ^2\Sigma^+$ $(v'=0)$ and $[a\ ^1\Delta]3d\delta\ ^2\Sigma^+$ $(v'=1)$ states is negligible. It might be argued that the actual interaction is not between $v'=0$ and $v'=1$ levels of the two states, but between vibrational levels with the same vibrational quantum number. In that case, however, we would have expected to observe the $[a\ ^1\Delta]3d\delta\ ^2\Sigma^+$ $(v'=0)$ as well as the $[b\ ^1\Sigma^+]4p\sigma\ ^2\Sigma^+$ $(v'=1)$ levels, contrary to our experiments. Moreover, the photoelectron spectra via the $[b\ ^1\Sigma^+]4p\sigma$ state should in that case have shown significant intensity in the $a\ ^1\Delta$ $(v^+=0)$ peak, and not only in the $a\ ^1\Delta$ $(v^+=1)$ channel.

The conclusion must be that at least one other state needs to be included in the interaction mechanism. We suspect that Rydberg-valence interactions affecting both the $[b\ ^1\Sigma^+]4p\sigma\ ^2\Sigma^+$ and $[a\ ^1\Delta]3d\delta\ ^2\Sigma^+$ states are at least partially responsible for the observations mentioned above. If one introduces a Rydberg-valence mixing involving at least one of the Rydberg states considered and the $[b\ ^1\Sigma^+]6\sigma^*$ valence state, the resulting potential energy curve(s) of the Rydberg state(s) will deviate from the anticipated one(s). Thus, by introducing Rydberg-valence mixing the Franck–Condon overlap term $(v'=0|v'=1)$ between the two $^2\Sigma^+$ states may not be small. From the observation that the $[a\ ^1\Delta]3d\delta\ ^2\Sigma^+$ $(v'=1)$ state has the smaller rotational constant of the two states in SH one might tentatively suggest that it has more valence character and thus is more affected by Rydberg-valence mixing. In agreement with this conclusion would be the paucity of rotational transitions [Fig. 8(c)], which presumably reflects the short-lived nature of this excited state due to predissociation.

In this section we have identified the $[b\ ^1\Sigma^+]4p\sigma\ ^2\Sigma^+$ $(v'=0)$ and the $[a\ ^1\Delta]3d\delta\ ^2\Sigma^+$ $(v'=1)$ Rydberg states of the SH and SD radicals. The complete assignment as $[b\ ^1\Sigma^+]4p\sigma\ ^2\Sigma^+$ $(v'=0)$ and $[a\ ^1\Delta]3d\delta\ ^2\Sigma^+$ $(v'=1)$ was based upon rotational analyses, isotopic shifts, quantum defects, and the determination of the ionic cores associated with these resonances. Inspection of the REMPI-PES spectra has revealed a substantial interaction between these states.

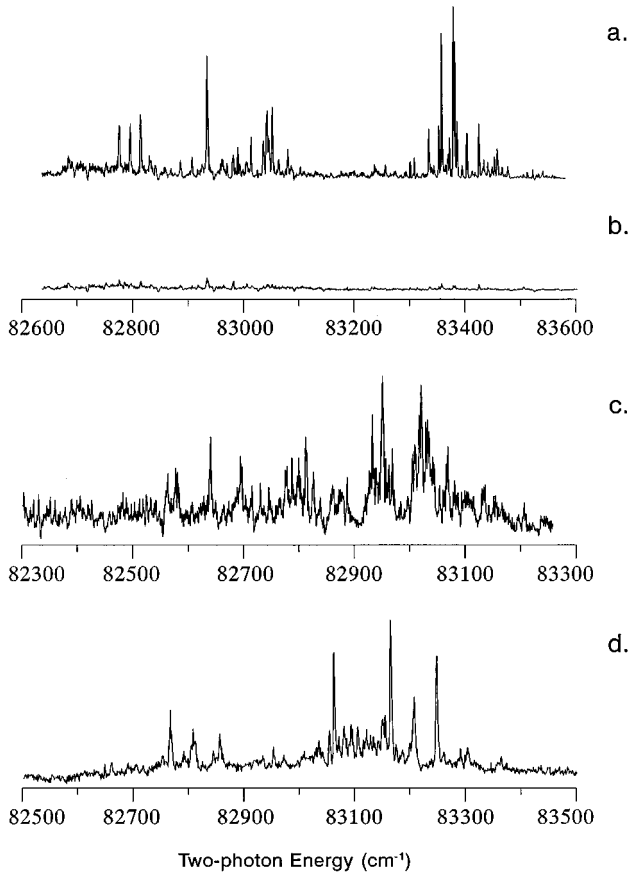

FIG. 10. Two-photon excitation spectrum of the $[b\ ^1\Sigma^+]4p\pi\ ^2\Pi\ (v'=0)\leftarrow\leftarrow X\ ^2\Pi\ (v''=0)$ transition in SH employing (a) linearly polarized excitation light, (b) circularly polarized excitation light. (c) Two-photon excitation spectrum of the $[b\ ^1\Sigma]4p\pi\ ^2\Pi\ (v'=0)\leftarrow\leftarrow X\ ^2\Pi\ (v''=0)$ transition in SD employing linearly polarized excitation light. (d) Two-photon excitation spectrum of the $[a\ ^1\Delta]5p\pi\ ^2\Pi\ (v'=0)\leftarrow\leftarrow X\ ^2\Pi\ (v''=0)$ transition in SD employing linearly polarized excitation light. All spectra were obtained with electron detection.

However, the two-state interaction model used seems to be an oversimplification. A description of the real situation would call for at least one other state to be involved in the interaction model.

D. Excitation spectra between 82 300 and 83 600 cm^{-1}

Figure 10(a) shows the two-photon excitation spectrum of SH in the energy range of 82 600–83 600 cm^{-1} obtained using linearly polarized radiation and monitoring only photoelectrons with a kinetic energy of about 2.7 eV. The same spectrum, but this time under circularly polarized conditions, is shown in Fig. 10(b). Obviously, the change in polarization results in a complete disappearance of the resonances.

The two-photon excitation spectrum of the SD radical in the same energy region and under the same experimental conditions as in Fig. 10(a) is depicted in Fig. 10(c). In SD a second excitation spectrum could be observed in this energy region by monitoring photoelectrons with a kinetic energy of about 3.8 eV [Fig. 10(d)]. Monitoring the same photoelectrons in SH resulted in a very sparse spectrum (not shown here) with only a few resonances at and around a one-photon energy of 41 500 cm^{-1}. As observed for SH, the SD resonances in Figs. 10(c) and 10(d) disappear completely by changing the polarization of the excitation laser from linear to circular.

Confirmation that all observed SH (SD) resonances do indeed derive from resonance enhancement at the two-photon level by states of the SH (SD) radical has been found by measuring excitation spectra with mass-resolved ion detection. These spectra, obtained by monitoring the SH^+ (SD^+) channel, are less well-resolved but do show resonances which correspond to the strongest lines in the spectra obtained by electron detection.

Although the excitation spectra shown in Fig. 10 are to a large extent rotationally resolved, the rotational analyses and the accompanying identification of rotational transitions appeared impossible. The polarization dependence of the two-photon excitation spectra demonstrates, however, that each SH (SD) spectrum is dominated by Q branches associated with the T_0^0 component of the two-photon transition tensor. This leads to the unambiguous conclusion that the transitions seen in Fig. 10(a) (SH) and Figs. 10(c) and 10(d) (SD) must derive their intensities from two-photon $^2\Pi\leftarrow\leftarrow{}^2\Pi$ transitions. We emphasize that for the SD radical two $^2\Pi\leftarrow\leftarrow{}^2\Pi$ transitions were observed, whereas for the SH radical only one transition and an indication for a second one were found.

Figure 11 displays photoelectron spectra obtained for (2+1) ionization of SH using several one-photon energies in the energy region of interest. From these spectra it becomes clear that a number of ionization channels are important. In Fig. 11(a), obtained at a one-photon energy of 41 695 cm^{-1}, ionization occurs predominantly into the vibrationless $b\ ^1\Sigma^+$ ionization continua as evidenced by the strong intensity of the photoelectron peak at ~2.7 eV. Figure 11(b), on the other hand, obtained at 41 495 cm^{-1}, shows that at this particular excitation energy ionization to the $a\ ^1\Delta\ (v^+=0)$ state, leading to 3.8 eV photoelectrons, is important.

The photoelectron spectra of Fig. 11 allow for a definite assignment of the ionic cores involved in both $^2\Pi\leftarrow\leftarrow{}^2\Pi$ transitions as the second ($a\ ^1\Delta$) and third ($b\ ^1\Sigma^+$) electronic state of the SH^+ ion. Figure 11 also shows that these ions are predominantly formed in their $v^+=0$ vibrational levels, although small peaks associated with ionization to vibrationally excited levels of the $a\ ^1\Delta$ and the $b\ ^1\Sigma^+$ ionic states are visible as well.

Further inspection of Fig. 11(a) shows three additional moderately intense peaks. The peak located at ~5.1 eV is visible in almost all of the recorded photoelectron spectra, and is in the energy region where (2+1) ionization of ground state SH, but also of S and H_2S is expected. Because the lowest ionization thresholds of these species[14,38,55] are nearly equal and therefore do not to allow for the separation of excitation spectra of the various species, we have monitored the excitation wavelength dependence of the integrated peak at ~5.1 eV. The spectrum obtained is dominated by transitions from the ^3P ground state of the sulfur atom to the

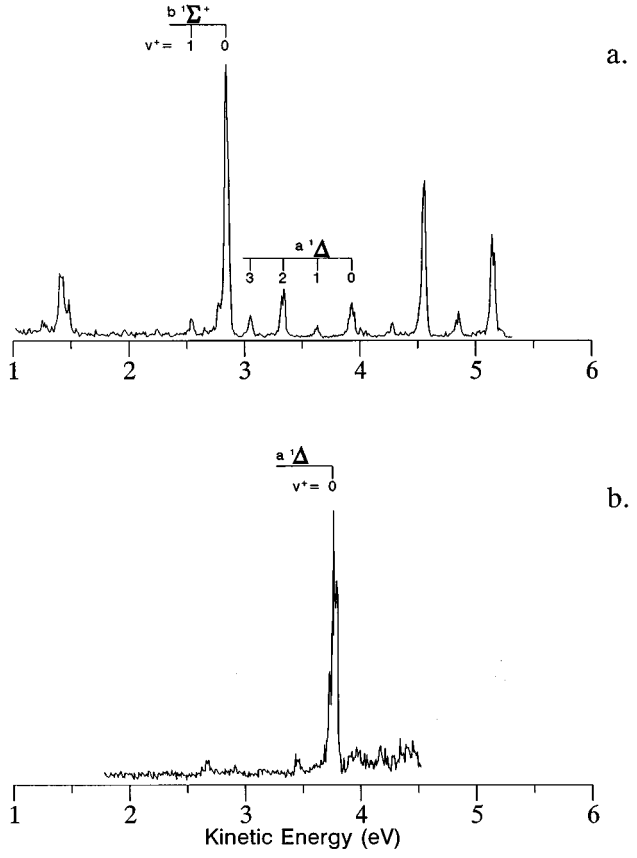

FIG. 11. Photoelectron spectra obtained for (2+1) ionization via (a) the $[b\ ^1\Sigma^+]4p\pi\ ^2\Pi$ ($v'=0$) state of SH using a one-photon energy of 41 695 cm^{-1}, (b) the $[a\ ^1\Delta]5p\pi\ ^2\Pi$ ($v'=0$) state of SH using a one-photon energy of 41 495 cm^{-1}.

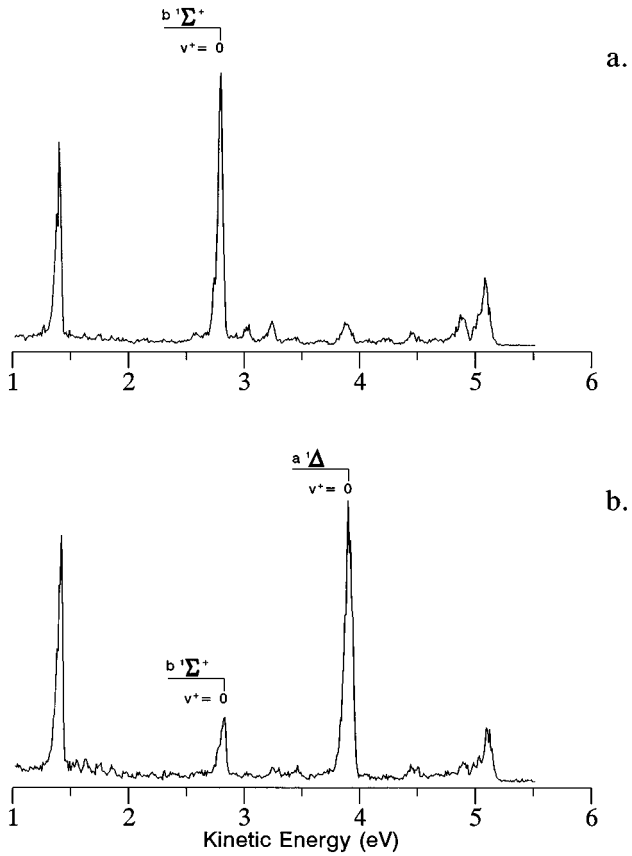

FIG. 12. Photoelectron spectra obtained for (2+1) ionization via (a) the $[b\ ^1\Sigma^+]4p\pi\ ^2\Pi$ ($v'=0$) state of SD using a one-photon energy of 41 516 cm^{-1}, (b) the $[a\ ^1\Delta]5p\pi\ ^2\Pi$ ($v'=0$) state of SD using a one-photon energy of 41 588 cm^{-1}.

$n=13-25$ members of the $(^4S°)np\ ^3P$ Rydberg series.[56] A careful inspection of the excitation spectrum also reveals low intensity resonance structures which show a close resemblance to the SH excitation spectrum displayed in Fig. 10(a). This observation indicates that ionization into the $X\ ^3\Sigma^-$ continua contributes to the ionization dynamics of the states under investigation. Apart from this moderately intense photoelectron peak, the photoelectron spectrum shown in Fig. 11(a) also displays a peak at ~4.8 eV of considerably lower intensity which can be identified as deriving from ionization to the $v^+=1$ level of the $X\ ^3\Sigma^-$ state.

Low kinetic energy photoelectrons of ~1.3 eV are present in all recorded photoelectron spectra. The excitation spectrum obtained by monitoring these slow photoelectrons shows some rotational structure superimposed on a continuous background. It is worth noting that similar low kinetic energy photoelectrons could also be observed in photoelectron spectra obtained at lower excitation energies, in particular in the energy region discussed in Sec. III C. Although it is not clear from which species these photoelectrons originate, we can definitely exclude the possibility that they are associated with resonance enhanced photoionization of SH. If they would derive from the SH radical, one would be forced to conclude that the (2+1) photoionization process from the $^2\Pi_{3/2}$ ground state spin–orbit component would involve ionization to rovibronic ionic limits ranging from 13.85 to 14.11 eV. It might be tempting to associate the latter value with the ionic limit of the $A\ ^3\Pi$ ionic state, since it agrees nicely with results from HeI VUV PES measurements.[12] The former value, however, is too small to be related to this ionic state, even if we would assume photoionization from the $^2\Pi_{1/2}$ ground state spin–orbit component to the lowest of the three different spin–orbit components of the $A\ ^3\Pi$ ionic state. Moreover, if the $A\ ^3\Pi$ ionic state would be involved, the photoelectron spectra would be expected to reveal three low kinetic energy photoelectron peaks associated with ionization to the three spin–orbit components of the $A\ ^3\Pi$ ionic state, instead of only one. An explanation in terms of photoionization from (vibrationally) excited states of SH can similarly be ruled out.

The third moderately intense peak deserving attention appears at ~4.5 eV and can be observed for example in Fig. 11(a). This peak is thought to be due to an impurity in the H_2S sample, most probably COS.

The examination of the photoelectron spectra obtained for (2+1) ionization of the SD radical (Fig. 12) allows us to identify in a similar way the photoelectrons which have selectively been monitored in obtaining Figs. 10(c) and 10(d).

These photoelectron spectra show that the SD^+ ions are dominantly formed in the $v^+=0$ vibrational level of the $b\ ^1\Sigma^+$ and the $a\ ^1\Delta$ ionic states. Photoelectron peaks which can be associated with vibrationally excited levels of the $a\ ^1\Delta$ and the $b\ ^1\Sigma^+$ ionic states are also visible in Fig. 12, but to a lesser extent. The SD REMPI-PES spectra show evidence as well for the formation of SD^+ ions in the $X\ ^3\Sigma^-$ ground ionic state, especially the $v^+=0$ and to a minor extent the $v^+=1$ vibrational level.

The excitation and photoelectron spectra discussed above show that the observed resonances must be associated with vibrationless transitions to two $^2\Pi$ Rydberg states built upon the $a\ ^1\Delta$ and $b\ ^1\Sigma^+$ ionic cores, respectively. We note, however, that the difference in excitation energies between the two isotopes (see Table II), seems somewhat larger than what has been observed for other $v'=0\leftarrow\leftarrow v''=0$ transitions in the present study. From Fig. 10(d) and the analogous spectrum for SH (not shown) we calculate quantum defects of 1.87 (SH) and 1.84 (SD) for $n=5$ with respect to the $a\ ^1\Delta$ ionic state. These quantum defects are somewhat large for a $5p$ Rydberg electron, but certainly do not point to a $4d$ or $5s$ orbital. Hence, the single-configuration description of this particular state is taken as $[a\ ^1\Delta]5p\pi\ ^2\Pi(v'=0)$. Analogously, Figs. 10(a) and 10(c) enable us to estimate the quantum defects of SH and SD with respect to the $b\ ^1\Sigma^+$ ionic state as 1.63 and 1.66, respectively, leading to$[b\ ^1\Sigma^+]4p\pi\ ^2\Pi(v'=0)$ as the appropriate single-configuration description.

The presence of two states of the same symmetry in an energy region which spans a mere 1000 cm^{-1} might suggest that a correct description of these states would go beyond the single-configuration approximation, because an interaction between the states should explicitly be taken into account. In this respect it is worthwhile to consider once again the excitation spectra, and compare them with those of the $[b\ ^1\Sigma^+]4p\sigma\ ^2\Sigma^+(v'=0)$ state (Sec. III C). In the excitation spectra of the latter state it was observed that the spectrum, in which the $b\ ^1\Sigma^+(v^+=0)$ ionization channel was monitored, is for all practical purposes equal to the spectrum obtained by monitoring the $a\ ^1\Delta(v^+=1)$ ionization channel. From this, and the observation of a nearby $[a\ ^1\Delta]3d\delta\ ^2\Sigma^+(v'=1)$ state we concluded that configuration interaction plays a significant role in the description of these states. For the states under investigation here a completely different behavior is observed, since the ionic-core resolved excitation spectra seem to be uncorrelated. This would point to a description in which the two states do not interact significantly, and consequently can exhibit more or less independent excitation spectra. On the other hand, the tentative conclusion that ionization to the $X\ ^3\Sigma^-$ ionization continua contributes to the ionization dynamics and that this channel seems to be correlated with the $b\ ^1\Sigma^+$ channel would suggest that it might be necessary to take another Rydberg state, built upon the ground $X\ ^3\Sigma^-$ ionic state, into account for a more appropriate description of the $[b\ ^1\Sigma^+]4p\pi\ ^2\Pi$ state.

In the previous sections we have concluded that Rydberg-valence mixing probably has a significant influence on the properties of the Rydberg states investigated. Here we find indications for such an influence as well in the unexpectedly weak transition to the $[a\ ^1\Delta]5p\pi\ ^2\Pi(v'=0)$ state of the SH radical. This observation presumably reflects the short-lived predissociative nature of the $^2\Pi$ state resulting from Rydberg-valence configuration interaction.

It is clear that on the basis of the spectra obtained in the present section merely qualitative arguments can be put forward. A detailed analysis of the interactions between all $^2\Pi$ states would at least require excitation spectra with a significantly higher signal to noise ratio which would allow for an unambiguous rotational assignment.

In this section we have discussed two newly observed $^2\Pi$ states of the SH (SD) radical, described by the $[a\ ^1\Delta]5p\pi$ and $[b\ ^1\Sigma^+]4p\pi$ configurations. An assignment of these states could be obtained by the polarization dependence of the excitation spectra, and by the REMPI-PES spectra. Despite their proximity, these two states do not seem to show a significant interaction. Indications for an interaction with dissociative valence states, on the other hand, feature more prominently.

E. Excitation spectra between 86 300 and 96 000 cm^{-1}

Figures 13(a) and 13(b) show wavelength scans of the SH radical obtained in two-photon energy regions exceeding the lowest ionization energy of the $X\ ^3\Sigma^-$ threshold of the SH^+ ion obtained using mass-resolved SH^+ ion detection. The resonant ion signal in Figs. 13(a) and 13(b) is superimposed upon a continuous background of SH^+ ions. These ions most probably derive from a direct two-photon ionization process of the $X\ ^2\Pi$ ground state of the SH radical, although they might also in part be generated via direct two-photon ionization of H_2S followed by one-photon photodissociation of H_2S^+.[57] Exactly the same excitation spectra are obtained when the S^+ channel, instead of the SH^+ channel, is monitored. However, the resonances do not show up in the H_2S^+ channel. The ion intensities in the S^+ and SH^+ channels are estimated to be more or less the same. Attempts to detect these MPI transitions by employing electron detection were not successful. Apart from an occasional (2+1) resonance originating from the ^3P ground state of the sulfur atom, and the omnipresent photoelectrons with kinetic energies of about 0.3–0.6 eV, no other electron signal could be detected. When excitation spectra are recorded monitoring the ''slow'' kinetic energy electrons of 0.3–0.6 eV, the resonances present in Figs. 13(a) and 13(b) could not be observed. These photoelectrons originate partly from direct two-photon ionization of SH, and partly from direct two-photon ionization of H_2S and atomic sulfur.

Excitation spectra of the SD radical in the same energy regions are displayed in Figs. 13(c) and 13(d). As for the lighter isotope, these transitions could only be observed employing mass-resolved ion detection. From the apparent small isotope shift in going from SH [Figs. 13(a) and 13(b)] to SD [Figs. 13(c) and 13(d)] it can be concluded that the vibrational quantum number does not change upon excitation, i.e., the excitations involve 0–0 transitions. Evidence

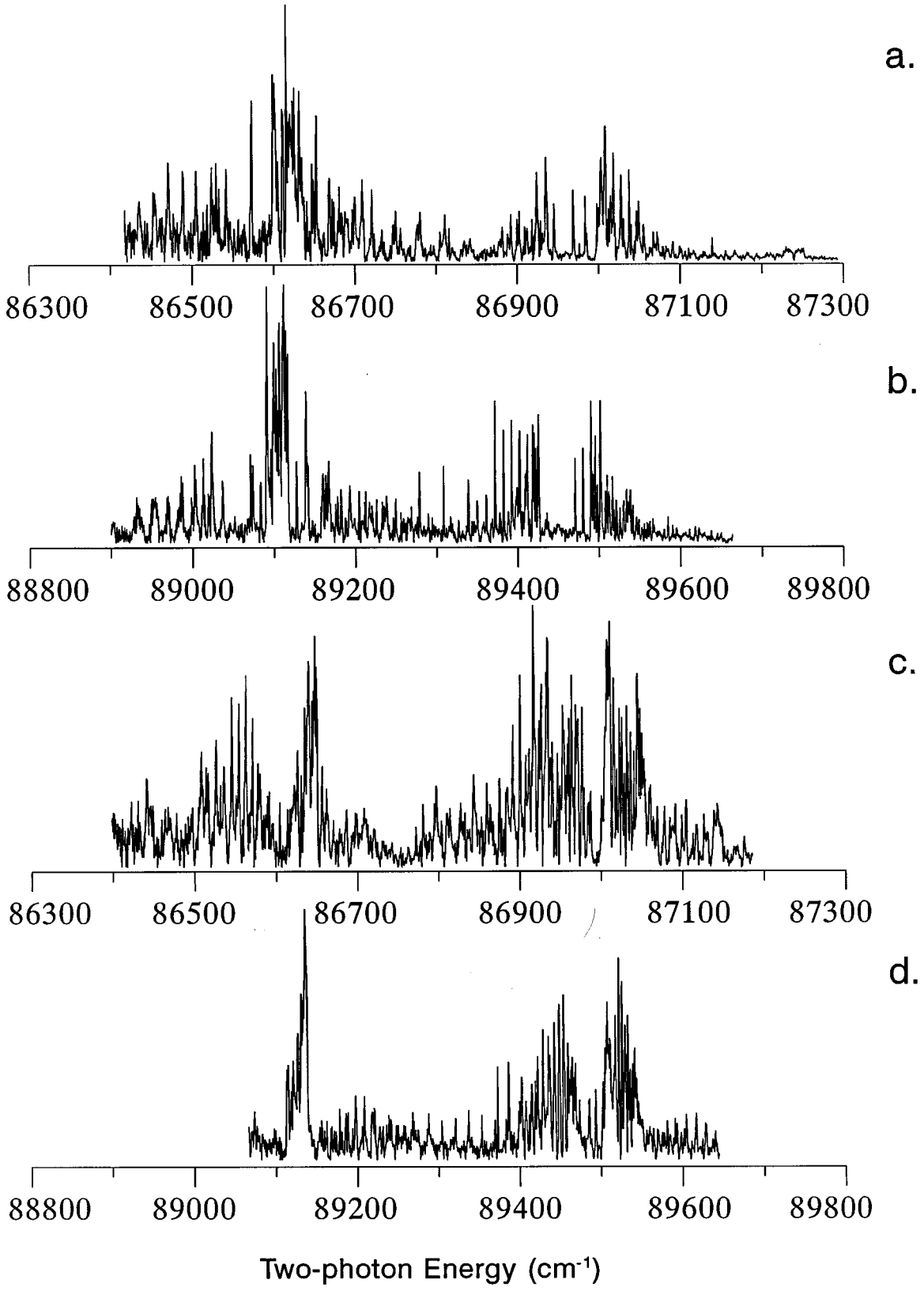

FIG. 13. Two-photon excitation spectra of (a) the $[a\ ^1\Delta]4d$ Rydberg complex of SH, (b) the $[a\ ^1\Delta]5d$ Rydberg complex of SH, (c) the $[a\ ^1\Delta]4d$ Rydberg complex of SD, and (d) the $[a\ ^1\Delta]5d$ Rydberg complex of SD. The spectra were obtained using mass-resolved ion detection and are corrected for the continuous background signal of SH^+ or SD^+ ions.

that resonant excitation takes place above the $X\ ^3\Sigma^-$ threshold at the two-photon level, rather than at the one-photon level, is found in the energy separation between the subbands seen in Figs. 13(a)–13(d). These energy separations correspond well with the spin–orbit splitting of the $X\ ^2\Pi$ ground state.

The spectra obtained for SH (SD) show a remarkable similarity, which would lead one to believe that they are successive members of the same Rydberg series. The rotational analyses of the excitation spectra have not proved feasible. Some insight concerning the assignment of these states can be obtained, however, by taking their excitation energies as the average of the energy positions of the subbands visible in the excitation spectra. From the effective quantum numbers thus calculated with respect to the $a\ ^1\Delta$ ionic state, $n^*=3.89$ [Figs. 13(a) and 13(c)] and $n^*=4.84$ [Figs. 13(b) and 13(d)], and the $b\ ^1\Sigma^+$ ionic state, $n^*=2.62$ [Figs. 13(a) and 13(c)] and $n^*=2.86$ [Figs. 13(b) and 13(d)], the similarity of the excitation spectra, and the autoionization characteristics of these states (*vide infra*), we conclude that they should be assigned to the $n=4$ [Figs. 13(a) and 13(c)] and $n=5$ [Figs. 13(b) and 13(d)] members of an nd Rydberg series converging upon the $a\ ^1\Delta$ ionic state. The $[a\ ^1\Delta]3d\pi\ ^2\Phi$ and $^2\Pi$ members of this Rydberg series have been discussed in Secs. III A and III B, respectively. Their excitation spectra have provided indications for l uncoupling. The mixing between the six different states deriving from the $[a\ ^1\Delta]nd\lambda$ configuration is expected to increase with n as the orbital angular momentum of the d electron will gradually decouple from the molecular axis. It follows that the bands observed in Figs. 13(a) and 13(b) might not be due to single states, but could rather consist of transitions to several Λ components of the $[a\ ^1\Delta]nd\lambda$ configurations. Compared to the spectra discussed in the previous sections, the excitation spectra exhibit a plethora of rotational lines. This can also be considered as an indication for the involvement of several transitions, rather than a single one. In this way, the difficulties encountered in analyzing these spectra can be rationalized.

The observation of rotationally resolved excitation spectra above the lowest ionization threshold, together with our inability to observe these transitions with electron detection, demonstrates that after two-photon excitation of these states the molecule does not ionize by the absorption of an extra photon into the $a\ ^1\Delta$, $b\ ^1\Sigma^+$, $A\ ^3\Pi$, or $c\ ^1\Pi$ electronically excited ionization continua of the SH^+ (SD^+) ion. Such a $(2+1)$ ionization process would be accompanied by photoelectrons with appropriate kinetic energies, but such high kinetic energy electrons could not be detected. On the other hand, the resonance enhancement seen in the SH^+ (SD^+) mass channel provides irrefutable evidence for ionization of the molecule after two-photon resonant excitation. A straightforward explanation for the presence of a resonant SH^+ (SD^+) ion signal and the absence of a $(2+1)$ electron signal would be that the two-photon resonant state autoionizes rapidly, leading to the formation of SH^+ (SD^+) ions in their $X\ ^3\Sigma^-$ ground state. Note that the photoelectrons deriving from this autoionization process have about the same kinetic energy as those resulting from a nonresonant two-photon ionization of S, SH, and H_2S. Probably, the autoionizing electron signal is so small in comparison with the enormous nonresonant background signal from these three species that its resonance enhancement cannot be observed. Employing SH^+ (SD^+) mass-resolved ion detection instead of electron detection enables us to reduce the background signal to that associated with one species, i.e., the SH^+ (SD^+) ion, a reduction which clearly allows for the observation of these MPI transitions.

Alternatively, the apparent absence of photoelectrons deriving from a $(2+1)$ photoionization process might be explained by a dissociative ionization process. Such a process would give rise to photoelectrons with a broad distribution of kinetic energies which probably cannot be distinguished from those deriving from the direct ionization processes. Such a mechanism would offer an explanation for the fact that we could detect the MPI transitions by monitoring the S^+ channel, which showed approximately the same intensity as that of the resonant SH^+ (SD^+) channel. Note, however, that the presence of resonant S^+ ions can equally well be explained by autoionization followed by one-photon (pre)dissociation of the $X\ ^3\Sigma^-$ ground ionic state of SH^+ (SD^+).[19] In our opinion dissociative photoionization is unlikely, since consideration of the relevant vertical transition energies[21] shows that a least two photons need to be absorbed from the Rydberg states to access dissociative ionic continua. We conclude that for the states whose excitation spectra are shown in Figs. 13(a)–13(d) autoionization dominates the overall ionization process. Decay into the underlying ionization continua of the $X\ ^3\Sigma^-$ ionic ground state is preferred over absorption of the extra photon needed for $(2+1)$ ionization.

In general, autoionization processes prevent the observation of rotationally resolved excitation spectra, as these processes lead to an extensive broadening of the rotational lines. Only a few examples of photoionization spectra are known in which autoionization, in particular spin–orbit autoionization, proceeds on a sufficiently slow time scale to allow for rotational resolution.[34,58–62] The linewidths and line shapes for such autoionizing Rydberg states are then clearly determined by the rate of autoionization. In the present study the lines of our Rydberg states have essentially the same widths as the lines of the Rydberg states discussed in the previous sections. The values obtained for the state shown in Fig. 13(a), when using the lowest possible laser power, vary from 0.60 to 0.90 cm^{-1}. Again we conclude that these linewidths are to a large extent determined by broadening effects. Apparently the autoionization rates for these states are not large enough to have a measurable influence on the linewidths under the present experimental conditions.

Apart from the rotationally well-resolved excitation spectra displayed in Figs. 13(a) and 13(b), we have also discovered four other bands above the lowest ionization energy of the $X\ ^3\Sigma^-$ threshold of the SH^+ ion. Excitation spectra of these four bands are depicted in Figs. 14(a)–14(d). Two of these bands, in Figs. 14(c) and 14(d), are not only situated above the $X\ ^3\Sigma^-$ threshold, but also above the first electronically excited threshold of the SH^+ ion ($a\ ^1\Delta$). The rotational

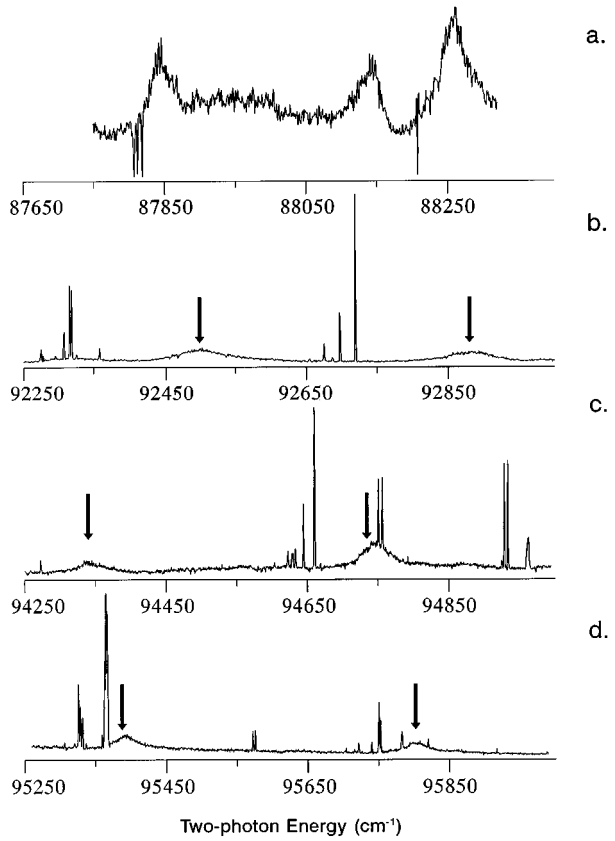

FIG. 14. Two-photon excitation spectra of (a) the $[b\ ^1\Sigma^+]3d$ Rydberg complex of SH, (b) the $[b\ ^1\Sigma^+]5p$ Rydberg complex of SH, (c) the $[b\ ^1\Sigma^+]4d$ Rydberg complex of SH, and (d) the $[b\ ^1\Sigma^+]4f$ Rydberg complex of SH: (a) was obtained using mass-resolved SH^+ ion detection, while for (b)–(d) electron detection was employed. The positions of the F_1 and F_2 transitions are indicated by the arrows in (b)–(d). The narrow lines in the spectra are due to transitions of the sulfur atom.

structure of these bands is no longer resolved and only the ground state spin–orbit splitting shows up as two subbands. Another difference between the Rydberg states observed in Figs. 13(a) and 13(b) and Figs. 14(a)–14(d) is that the latter MPI transitions can be detected by employing electron detection as well. The spectra depicted in Figs. 14(b)–14(d) were obtained by monitoring photoelectrons which derive from autoionization into the continua of the $X\ ^3\Sigma^-$ state after two-photon resonant excitation. This two-photon resonant electron signal is superimposed on the direct ionization background signal of H_2S, SH, and atomic sulfur. In contrast to the situation described for the Rydberg states shown in Fig. 13, this resonant electron signal is large enough to be distinguished from the enormous nonresonant background signal. The narrow lines observed in Figs. 14(a)–14(c) can all be assigned to two-photon atomic sulfur resonances. Most of them agree with transitions to Rydberg states previously investigated,[63] while others will be the subject of a forthcoming article.[56] These two-photon resonant states are located above the ground $^4S°$ ionic state of sulfur, and were excited in the present experiments from the ^3P ground state. Autoionization of these states results in the formation of atomic sulfur ions in the $^4S°$ ionic ground state and photoelectrons with more or less the same kinetic energy as those derived from the autoionization process of the SH radical. This similarity in kinetic energies explains the presence of atomic sulfur resonances in Figs. 14(b) and 14(c). Note that the wavelength scan of Fig. 14(a) was obtained by monitoring the SH^+ ion channel. The presence of atomic sulfur resonances in this spectrum is due to strong sulfur resonances in the S^+ ion channel. Cross talk between the S^+ and SH^+ channels gives rise to a negative baseline shift in the SH^+ ion channel. As the states depicted in Fig. 14 exhibit evidence for lifetime broadening, it is clear that their autoionization rates are much faster than those of the states depicted in Fig. 13.

Similar to the procedure employed for the assignment of the states responsible for the resonance enhancement in Figs. 13(a)–13(d), we can assign the excitation spectra of Figs. 14(a) and 14(c) to the $n=3$ ($n^*=2.73$) and $n=4$ ($n^*=3.68$) successive members of an nd Rydberg series converging upon the $b\ ^1\Sigma^+$ ionic state. Likewise, the broad transitions in Figs. 14(b) and 14(d) can be attributed to $[b\ ^1\Sigma^+]5p$ ($n^*=3.33$) and $[b\ ^1\Sigma^+]4f$ ($n^*=3.93$) resonances, respectively. The $4p\sigma$ and $4p\pi$ members of the $[b\ ^1\Sigma^+]np$ series have been dealt with in Secs. III C and III D, respectively. As discussed before for the assignments of the $[a\ ^1\Delta]4d$ and $5d$ Rydberg complexes, the bands observed in Figs. 14(a)–14(d), are most probably not due to single states, but rather to transitions to several Λ components of the $[b\ ^1\Sigma^+]nd\lambda$, $[b\ ^1\Sigma^+]5p\lambda$, and $[b\ ^1\Sigma^+]4f\lambda$ configurations.

The above assignments relate rotationally resolved excitation spectra above the $X\ ^3\Sigma^-$ ionization threshold to Rydberg states converging to the $a\ ^1\Delta$ ionic limit and rotationally unresolved excitation spectra to Rydberg states converging to the $b\ ^1\Sigma^+$ ionic limit. Another possible assignment for the rotationally resolved excitation spectra and the spectrum depicted in Fig. 14(a) would be to attribute them to different Λ components of the $[b\ ^1\Sigma^+]3d\lambda$ configuration. Employing the first assignment, we need to rationalize the difference in lifetimes by considering the electronic character of the Rydberg states, i.e., Rydberg states would autoionize slower if they converge to the $a\ ^1\Delta$ ionic limit, rather than to the $b\ ^1\Sigma^+$ ionic limit. Employing the second option would mean that we should invoke very different autoionization rates for the $^2\Sigma^+$, $^2\Pi$, and $^2\Delta$ Rydberg states belonging to the $[b\ ^1\Sigma^+]3d\lambda$ configuration. Although on the basis of the calculated effective quantum numbers we cannot exclude the last assignment, we tend to favor the former one because previous experiments have provided evidence for long lifetimes of Rydberg states with an $a\ ^1\Delta$ ionic core.[14,34,59] First, the photoionization spectrum of the OH radical shows bands with sharp rotational structure,[59] which were tentatively assigned to several members of an nd Rydberg series converging upon the $a\ ^1\Delta$ excited ionic state of OH^+. Second, the results of recent ZEKE-PFI experiments on the $a\ ^1\Delta$ ionic state of the SH (SD) radical have revealed that high-n Rydberg states with an $a\ ^1\Delta$ ionic core are relatively insensitive to autoionization processes.[14] Finally, a (2+1) REMPI-PES study on the $[a\ ^1\Delta]5p\pi\ ^2\Phi$ Rydberg state of the SH (SD) radical has indicated that this state shows very unusual

behavior.[34] Although its excitation energy exceeds the lowest ionization threshold, rotationally well-resolved excitation spectra were obtained. Moreover, this study has revealed that for this particular state autoionization processes play such a minor role, that after excitation of the $[a\ ^1\Delta]5p\pi\ ^2\Phi$ state the molecule is dominantly ionized by absorption of an additional photon.

As yet we have paid no attention to what kind of autoionization processes might be involved here. In principle, the states built upon the $a\ ^1\Delta$ or $b\ ^1\Sigma^+$ ionic core are coupled to the ionization continua of the lower-lying $X\ ^3\Sigma^-$ ionic ground state via off-diagonal matrix elements, which originate from the electrostatic part ($\Sigma e^2/r_{ij}$) of the Hamiltonian, i.e., such states should be subject to electrostatic autoionization processes leading to an ion in its $X\ ^3\Sigma^-$ ground state and a free electron. We have tried to obtain a qualitative impression of these interaction elements by using Slater determinants for discrete state and final-state continua wave functions, and by writing the electrostatic part ($\Sigma e^2/r_{ij}$) as a sum over the product of spherical harmonics. Such qualitative considerations, however, do not seem to support the idea that there are significant differences in the autoionization rates for states built upon the $a\ ^1\Delta$ or $b\ ^1\Sigma^+$ ionic cores. The bands shown in Figs. 14(c) and 14(d) are not only situated above the $X\ ^3\Sigma^-$ threshold, but also above the $a\ ^1\Delta$ threshold. These states, which have been assigned as converging upon the $b\ ^1\Sigma^+$ ionic state, can not only autoionize into the $X\ ^3\Sigma^-$ ionic continua, but into the $a\ ^1\Delta$ continua as well. Despite the availability of this extra electrostatic decay channel, the states observed in Figs. 14(c) and 14(d) do not appear much different from those displayed in Figs. 14(a) and 14(b) to which only the $X\ ^3\Sigma^-$ channel is available. Taking this into consideration we feel that electrostatic autoionization has limited importance. A more realistic alternative explanation for the difference in autoionization rates might be found in the involvement of spin–orbit interaction. The $X\ ^3\Sigma^-$ ground ionic state and the $a\ ^1\Delta$ and $b\ ^1\Sigma^+$ excited ionic states all derive from the $\cdots(5\sigma)^2(2\pi)^2$ configuration. The $X\ ^3\Sigma^-$ and $b\ ^1\Sigma^+$ ionic states can interact via off-diagonal matrix elements of the spin–orbit Hamiltonian, but such matrix elements are zero for the interaction between the $a\ ^1\Delta$ and $X\ ^3\Sigma^-$ states. Consequently, Rydberg states built upon the $b\ ^1\Sigma^+$ ionic core can be considered as having some $X\ ^3\Sigma^-$ ionic character, leading to their relatively strong coupling to the ionization continua of the $X\ ^3\Sigma^-$ ground state. Presently, high-quality *ab initio* calculations are in progress, which should put these ideas on a quantitative basis.

In this section we have observed six states with excitation energies exceeding the lowest ionization threshold. Two states display rotationally resolved excitation spectra, whereas the other spectra show clear evidence of lifetime broadening. The differences have been attributed to different autoionization rates for Rydberg states converging to the $a\ ^1\Delta$ and the $b\ ^1\Sigma^+$ ionic states.

ACKNOWLEDGMENTS

The authors thank C. M. Western (Bristol), J. G. Snijders (Amsterdam), and H. Lefebvre-Brion (Orsay), for helpful discussions. The financial support from the Netherlands Organization for Scientific Research (N.W.O.) is gratefully acknowledged. J.B.M. thanks N.W.O. for a bursary for a stay at the University of Bristol.

[1] K. Sinha, Proc. Astron. Soc. Austr. **9**, 32 (1991).
[2] C. K. Walker, C. J. Lada, E. T. Young, P. R. Maloney, and B. A. Wilking, Astrophys. J. **309**, L47 (1986).
[3] S. Saito, K. Kawaguchi, S. Yamamoto, M. Ohishi, H. Suzuki, and N. Kaifu, Astrophys. J. **317**, L115 (1987).
[4] S. Yamamoto, S. Saito, K. Kawaguchi, N. Kaifu, H. Suzuki, and M. Ohishi, Astrophys. J. **317**, L119 (1987).
[5] M. L. Meeks, M. A. Gordon, and M. M. Litvak, Science **163**, 173 (1969).
[6] C. E. Heiles and M. B. E. Turner, Astrophys. Lett. **8**, 89 (1971).
[7] S. H. Ashworth and J. M. Brown, J. Mol. Spectrosc. **153**, 41 (1992).
[8] R. S. Ram, P. F. Bernath, R. Engleman, and J. W. Brault, J. Mol. Spectrosc. **172**, 34 (1995), and references therein.
[9] G. Porter, Discuss. Faraday Soc. **9**, 60 (1950).
[10] D. A. Ramsay, J. Chem. Phys. **20**, 1920 (1952).
[11] J. W. C. Johns and D. A. Ramsay, Can. J. Phys. **39**, 210 (1961).
[12] S. J. Dunlavey, J. M. Dyke, N. K. Fayad, N. Jonathan, and A. Morris, Mol. Phys. **38**, 3 (1979); **44**, 265 (1981).
[13] C. W. Hsu, D. P. Baldwin, C. L. Liao, and C. Y. Ng, J. Chem. Phys. **100**, 8047 (1994).
[14] J. B. Milan, W. J. Buma, and C. A. de Lange, J. Chem. Phys. **104**, 521 (1996).
[15] P. R. Brown, P. B. Davies, and S. A. Johnson, Chem. Phys. Lett. **132**, 582 (1986).
[16] D. C. Hovde and R. J. Saykally, J. Chem. Phys. **87**, 4332 (1987).
[17] M. Horani, S. Leach, and J. Rostas, J. Mol. Spectrosc. **23**, 115 (1967).
[18] J. Rostas, M. Horani, J. Brion, D. Daumont, and J. Malicet, Mol. Phys. **52**, 1431 (1984).
[19] E. P. Edwards, C. S. Maclean, and P. J. Sarre, Mol. Phys. **52**, 1453 (1984).
[20] A. P. Levick and P. J. Sarre, J. Mol. Spectrosc. **133**, 227 (1989).
[21] J. K. Park and H. Sun, Chem. Phys. Lett. **194**, 485 (1992), and references therein.
[22] B. A. Morrow, Can. J. Phys. **44**, 2447 (1966).
[23] M. N. R. Ashfold, B. Tutcher, and C. M. Western, Mol. Phys. **66**, 981 (1989).
[24] P. J. Bruna and G. Hirsch, Mol. Phys. **61**, 1359 (1987).
[25] L. C. Lee, X. Wang, and M. Suto, J. Chem. Phys. **86**, 4353 (1987).
[26] W. G. Hawkins and P. L. Houston, J. Chem. Phys. **73**, 297 (1980); **76**, 729 (1982).
[27] Z. Xu, B. Koplitz, and C. Wittig, J. Chem. Phys. **87**, 1062 (1987).
[28] B. R. Weiner, H. B. Levene, J. J. Valentini, and A. P. Baronavski, J. Chem. Phys. **90**, 1403 (1989).
[29] X. Xie, L. Schnieder, H. Wallmeier, R. Boettner, K. H. Welge, and M. N. R. Ashfold, J. Chem. Phys. **92**, 1608 (1990).
[30] R. E. Continetti, B. A. Balko, and Y. T. Lee, Chem. Phys. Lett. **182**, 400 (1991).
[31] M. N. R. Ashfold, L. Schnieder, and K. H. Welge, Faraday Discuss. Chem. Soc. **91**, 128 (1991).
[32] G. P. Morley, I. R. Lambert, D. H. Mordaunt, S. H. S. Wilson, M. N. R. Ashfold, R. N. Dixon, and C. M. Western, J. Chem. Soc. Faraday Trans. **89**, 3865 (1993).
[33] G. N. A. Veen, K. A. Mohamed, T. Baller, and A. E. de Vries, Chem. Phys. **74**, 261 (1993).
[34] J. B. Milan, W. J. Buma, C. A. de Lange, C. M. Western, and M. N. R. Ashfold, Chem. Phys. Lett. **239**, 326 (1995).
[35] J. B. Milan, W. J. Buma, C. A. de Lange, K. Wang, and V. McKoy, J. Chem. Phys. **103**, 3262 (1995).
[36] M. R. Dobber, W. J. Buma, and C. A. de Lange, J. Chem. Phys. **101**, 9303 (1994).
[37] C. E. Moore, *Atomic Energy Levels*, Natl. Stand. Ref. Data. Ser. Natl. Bur. Stand. 35 (U.S. GPO, Washington, D.C., 1971).
[38] W. C. Martin, R. Zulubas, and A. Musgrove, J. Phys. Chem. Ref. Data **19**, 820 (1990).
[39] J. M. Brown, M. Kaise, C. M. L. Kerr, and D. J. Milton, Mol. Phys. **36**, 553 (1978).
[40] R. N. Dixon, J. M. Bayley, and M. N. R. Ashfold, J. Chem. Phys. **84**, 21 (1984).

[41] P. A. Freedman, Can. J. Phys. **55**, 1387 (1977).
[42] S. T. Pratt, Ch. Jungen, and E. Miescher, J. Chem. Phys. **90**, 5971 (1989).
[43] A. Vient, N, Shafizadeh, J. H. Fillion, D. Gauyacq, M. Horani, and J. L. Lemaire, J. Phys. Chem. **99**, 1666 (1995).
[44] R. A. Gottscho, J. B. Koffend, R. W. Field, and J. R. Lombardi, J. Chem. Phys. **68**, 4110 (1978).
[45] K. P. Huber and F. Alberti, J. Mol. Spectrosc. **97**, 387 (1983).
[46] F. Alberti, K. P. Huber, and E. C. Looi, J. Mol. Spectrosc. **102**, 289 (1983).
[47] D. Cossart, C. Cossart-Magos, M. Vervloet, and T. Bergeman, J. Mol. Spectrosc. **163**, 587 (1994).
[48] F. Rostas, F. Launay, M. Eidelsberg, M. Benharrous, C. Blaess, and K. P. Huber, Can. J. Phys. **72**, 913 (1994).
[49] J. Ishii, K. Uehara, and K. Tsukiyama, J. Chem. Phys. **102**, 9174 (1995).
[50] K. Wang, V. McKoy, J. B. Milan, W. J. Buma, and C. A. de Lange (unpublished).
[51] C. A. Mayhew, J. P. Connerade, M. A. Biag, M. N. R. Ashfold, J. M. Bayley, R. N. Dixon, and J. D. Prince, J. Chem. Soc. Faraday Trans. **83**, 417 (1987).
[52] J. Czarny, P. Felenbok, and H. Lefebvre-Brion, J. Phys. B **4**, 124 (1971).
[53] K. Yoshino and D. E. Freedman, J. Mol. Spectrosc. **76**, 153 (1979).
[54] J. Baker, J. L. Lemaire, S. Couris, A. Vient, D. Malmasson, and F. Rostas, Chem. Phys. **178**, 569 (1994).
[55] I. Fischer, A. Lochschmidt, A. Strobel, G. Niedner-Schatteburg, K. Müller-Dethlefs, and V. E. Bondybey, J. Chem. Phys. **98**, 3592 (1993).
[56] S. Woutersen, J. B. Milan, W. J. Buma, and C. A. de Lange, Phys. Rev. A (in press).
[57] Y. Achiba, K. Sato, K. Shobatake, and K. Kimura, J. Chem. Phys. **77**, 2709 (1982).
[58] P. M. Dehmer and W. A. Chupka, J. Chem. Phys. **80**, 1030 (1984).
[59] P. M. Dehmer, Chem. Phys. Lett. **110**, 79 (1984).
[60] A. Mank, M. Drescher, T. Huth-Fehre, N. Böwering, U. Heinzmann, and H. Lefebvre-Brion, J. Chem. Phys. **95**, 1676 (1991).
[61] M. Drescher, A. Brockhinke, N. Böwering, U. Heinzmann, and H. Lefebvre-Brion, J. Chem. Phys. **99**, 2300 (1993), and references therein.
[62] N. P. L. Wales, W. J. Buma, C. A. de Lange, and H. Lefebvre-Brion, J. Chem. Phys. **105**, 2978 (1996).
[63] S. T. Pratt, Phys. Rev. A **38**, 1270 (1988).